ELECTROCHEMICAL METAL DEPOSITION CONTROLLED BY MOLECULAR ASSEMBLIES

Enrico Bartoletti

A Thesis Submitted for the Degree of MPhil
at the
University of St Andrews

2015

UNIVERSITY OF ST. ANDREWS

SCHOOL OF CHEMISTRY

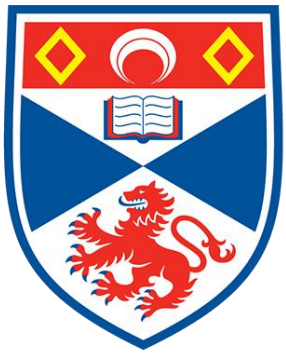

ELECTROCHEMICAL METAL DEPOSITION CONTROLLED BY MOLECULAR ASSEMBLIES

(MPHIL THESIS)

ENRICO BARTOLETTI

SUPERVISED BY

PROFESSOR MANFRED BUCK

SEPTEMBER 2015

I, Enrico Bartoletti, hereby certify that this thesis, which is approximately 16000 words in length, has been written by me, and that it is the record of work carried out by me, or principally by myself in collaboration with others as acknowledged, and that it has not been submitted in any previous application for a higher degree.

I was admitted as a research student in September 2013 and as a candidate for the degree of Chemistry in 2015; the higher study for which this is a record was carried out in the University of St Andrews between 2013 and 2015.

I hereby certify that the candidate has fulfilled the conditions of the Resolution and Regulations appropriate for the degree of Chemistry in the University of St Andrews and that the candidate is qualified to submit this thesis in application for that degree.

In submitting this thesis to the University of St Andrews I understand that I am giving permission for it to be made available for use in accordance with the regulations of the University Library for the time being in force, subject to any copyright vested in the work not being affected thereby. I also understand that the title and the abstract will be published, and that a copy of the work may be made and supplied to any bona fide library or research worker, that my thesis will be electronically accessible for personal or research use unless exempt by award of an embargo as requested below, and that the library has the right to migrate my thesis into new electronic forms as required to ensure continued access to the thesis. I have obtained any third-party copyright permissions that may be required in order to allow such access and migration, or have requested the appropriate embargo below.

The following is an agreed request by candidate and supervisor regarding the publication of this thesis:

Embargo on all or part of print & electronic copies for a period of 2 years on the following grounds:

- Publication would be commercially damaging to the researcher, or to the supervisor, or the University
- Publication would preclude future publication

ABSTRACT

This thesis studies the electrochemical deposition of the metals Pd and Cu on self-assembled monolayers (SAMs) formed on Au substrates. The SAMs are composed of aromatic mercaptans like 4,4′-dipyridyl disulfide or 3-(4-pyridine-4-ylphenyl)propane-1-thiol which are able to coordinate metal ions at their outer surface of the layer. Through an electrochemical reduction metal is deposited on top of the SAM thus, generating a Metal/SAM/Metal sandwich-like structure. Different outcomes arise, since the use of Pd coordinated to the SAM causes the formation of nanoparticles of limited size on top of the organic layer, while the use of Cu electrolyte elicits the formation of normal nanoisland growth. Also experiments in which both Cu and Pd were present at the same time are performed and by this means mixed nanoparticles on top of the organic layer are generated. The structures are created and analysed by cyclic voltammetry. The system in which only Cu is involved shows a potentially unlimited growth of bulk Cu, while the systems in which only Pd is involved or mixed Cu/Pd nanoparticles are created display a self-limiting growth which may be of great interest because it allows the precise tailoring of nanostructures.

This thesis studies also the development of patterned structures achieved through chronoamperometric experiments: a substrate is half-immersed in a $PdSO_4$ solution which selectively coordinates Pd to one part of the SAM. Reduction of the Pd in the presence of Cu electrolyte results in a selective deposition of Cu on the Pd seeded area of the SAM. This procedure allows for a quick, easy and reliable way to create deposition patterns with a cheap setup. The samples are characterised by optical microscopy, scanning electron microscopy and atomic force microscopy.

ACKNOWLEDGEMENTS

In first instance I would like to thank professor Manfred Buck for allowing me to fulfil this research project under his supervision and for his support in giving me useful expertise during this MPhil.

In addition I want to thank my labmates Angus Ritchie, Nikolaus Meyerbröker, Hannah Aitchison, Baharan Karamzadeh, Henry Chandler and Ross Irvine for their daily support.

A general acknowledgement to St Andrews staff for their technical and social support.

Summary

1 Introduction

1.1 SAMs architecture

There are molecules that today have a paramount importance because, if they are exposed to the right surface, they organize themselves to form an ordered structure. Such a layer, which assembles by itself, is called Self-Assembled Monolayer (SAM). The properties of regularity determine a molecular architecture that nowadays is very sought-after by modern chemistry to create useful structures in the nano-range. One of the most common examples of this kind is the self-assembly of thiols onto a Au surface. Thiols are important because the quality of the respective SAMs is very high. Good results can be achieved not only with thiols, but also with other sulfur-containing molecules like organic sulfides and organic disulfides adsorbed on noble metal surfaces. Pd, Pt, Cu and Ag show quite good suitability as substrates for SAMs as well, but Au is the best metal for this kind of use, because it is the least oxidizable, the inertest, it is available with high purity and relative scarcity of topographic defects. Furthermore the unique affinity Au has towards sulfur-containing compounds allows formation of SAMs of very good quality.[1] Thiols are organic molecules that are the sulfur analogue of alcohols, that is, they possess a -SH group, in general in a terminal part of the molecule. From an inorganic chemistry point of view, according to Pearson's theory,[2] thiolates, which derive from deprotonation of thiols, are soft bases, that is, they react in a basic way mainly towards chemical compounds whose charge-to-volume ratio is low, like Au itself. This is supported by a considerable number of articles that conclude the formation of the complex shown in Figure 1 which involves the elimination of H_2 from the interface.[3,4,5,6] Similar considerations hold for sulfides and disulfides, that are organic compounds that encompass the groups -S- and -S-S-, respectively (Figure 2). In the case of sulfides the difference with thiols is that the carbon-sulfur bond is not split and conformational requirements due to the bond with the substrate might disfavour efficient packing.[7,8] Disulfides, instead, break at the sulfur-sulfur bond and get reduced, forming thiolates.[9] Thiols used as SAM precursors are composed of a head group that binds to the substrate and anchors the whole structure to it, a linker that connects the head group to the tail group and the tail group itself, that can be functionalized or not, depending on the general use of the SAM. In absence of the Au surface, thiols do not self-assemble because dispersion forces that act between different chains are not sufficiently strong (on the order of 1.0 kcal/mol per methylene group[10]) to hold a thiol sheet together. Conversely, because the sulfur-gold bond is significantly stronger (around 45 kcal/mol[11]), molecules effectively bind to the surface and lateral interactions among

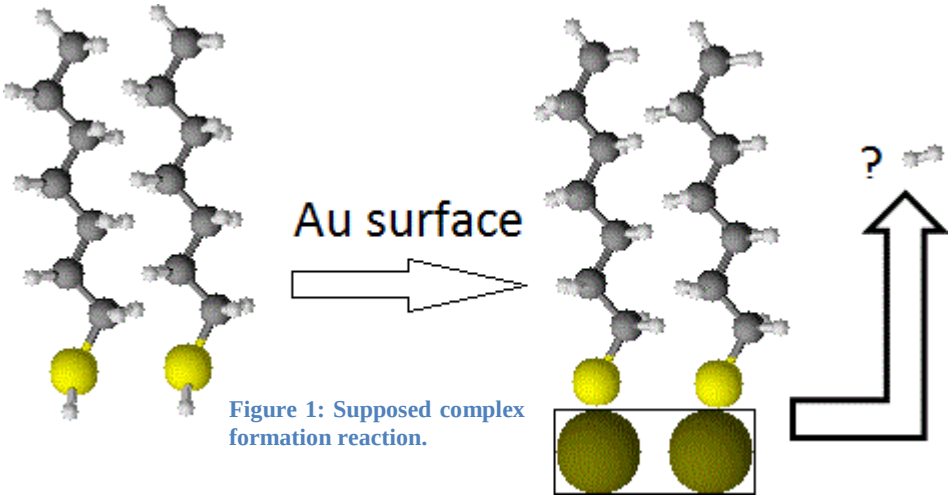

Figure 1: Supposed complex formation reaction.

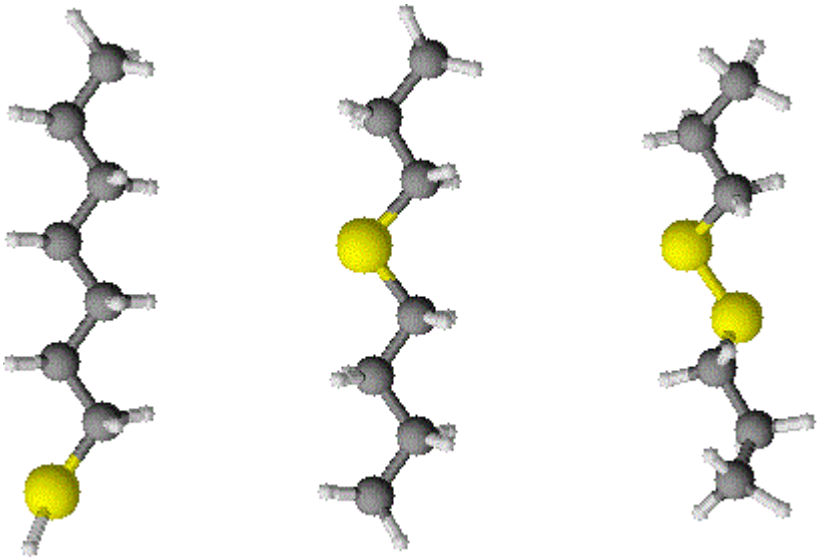

Figure 2: Various sulfur compounds, from left to right, thiol, sulfide and disulfide.

chains can quite straightforwardly approach the molecules to each other, until a thiol aggregate, that is, a SAM, is built up. The SAM, therefore, tends to maximize the interactions with the Au substrate and the interactions between thiol molecules, but overall the gold-sulfur bond is the major driving force for the construction of the SAM. The linker of the thiol may be an alkane chain which can be even quite long (sometimes beyond 20 carbon atoms). Chains like these are rather flexible, and this is, for example, relevant for the application of thiol SAMs in the electrodeposition of metals, as it makes the layers penetrable for metal ions.[12] Conversely, if the linker of the thiol consists of one or more benzene rings or a similar type of ring, the overall structure will be much stiffer and penetration will occur to a lesser extent.[13]

1.2 Surface modification and functionalization

A tail group can be an inert -CH_3 moiety with no particular function, or it can be a functional group depending on the application of the SAM: for example, an amine tail group can make the SAM prone to bind, via elimination of a water molecule, to perfluorinated compounds that end with a carboxylic moiety to obtain a highly hydrophobic surface (see Figure 3).[14] Pyridine, which is of particular relevance for this work, can coordinate metal ions like Pd or Cu, that in turn can be manipulated, for example through reduction to neutral atoms that form a metallic layer or nanoparticles. This illustrates that the tail group allows the tailoring of surface properties. Adsorption is limited to a monolayer (as the acronym suggests) because interaction between the tail group of the base layer and possibly additional SAM-forming molecules is such that multilayer formation does not occur. Moreover, SAMs tend to be quite well-ordered, which is favourable when exploiting their mechanical, electronic or

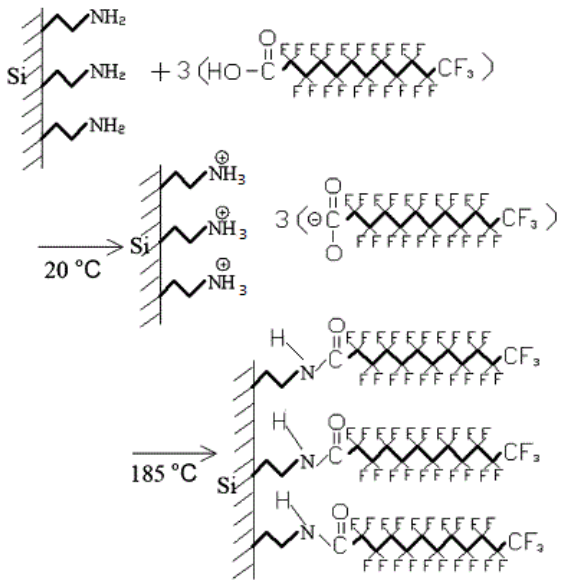

Figure 3: Functionalization of a surface with a perfluorinated molecule to obtain a hydrophobic structure by elimination of water (not shown in the picture). Figure adapted from reference 14.

electrochemical properties.[15,16,17] For several kinds of thiols like 4,4'-biphenyldithiol, 1-tetradecanethiol and 1-hexadecanethiol, experiments of nanoindentation have demonstrated good resistance to tip penetrating also at the nanoscale.[15] The linear dependence between the overpotential applied to the electronic system and the logarithm of the current has been confirmed either for SAMs composed of alkane thiols or for SAMs composed of aromatic thiols, in both cases without a functionalized tail group.[16] Even SAMs composed of a molecule as simple and common as sodium oleate have shown interesting electrochemical properties, by enhancing the corrosion resistance of mild steel in saline water. Because of its wide availability, oleic acid or its salts can be potentially used as economical passivating film precursors in the future.[17]

1.3 SAMs formation thermodynamics and kinetics

SAMs are conveniently prepared by immersing a substrate in a SAM-precursor solution for a predetermined time (often overnight). Thiols, and also sulfides and disulfides, are mildly polar chemical species. Thus, they are in general not well soluble in water and polar solvents. Long hydrocarbons show better solubility but kinetically hinder the release of SAM-precursors so strongly that formation of a proper SAM from them is troublesome.[18] Therefore short hydrocarbons or alcohols are usually chosen. However, the former might yield a lower degree of organization in the SAM, while alcohols do not show this problem.[19,20] Therefore ethanol is chosen most of the time, also because it is attainable in high purity and has a low price. It is to be reminded that the time necessary to achieve a good coverage, and, subsequently, a good SAM, is inversely proportional to the concentration of the thiol.[19,21] This fact is intuitive, because the time required to achieve full coverage is defined by the flux of the molecules onto the surface. However, the kinetics is not the same throughout the whole film formation process, because the process is dominated at the beginning by thiols attaching to the surface, then by the trend of molecules to pack along each other in a quite disordered manner, and finally by the steric rearrangement of the chains that compose the SAM.[22,23] All these stages are intrinsically different, and may even happen at the same time in different areas of the sample because of unavoidable heterogeneities of the sample surface.

Intermolecular interactions are also important from the thermodynamic point of view: the stronger they are, the more robust the formed SAM is. For alkane thiols this means that the SAM strength depends heavily on the length of the chain, because the more methylene units interact through dispersion interactions, the more stable the layer will be. Thiols whose linker consists of aromatic units follow a similar rule: the more rings the SAM has, the harder it is to be destroyed. This rule is based on considerations analogous to the ones that hold for alkane thiols: if more rings contribute to stabilize the overall SAM through dispersion interactions, the SAM itself will be more robust. A test of the toughness of a SAM can be performed by thermal means: SAMs composed of long chains desorb at higher temperatures than SAMs composed of short chains.[24] Furthermore, under electrochemically reducing conditions, the potential at which the molecules desorb depends on the length of the molecule even though the Au-S bond contributes most to the SAM stability.[25] It is noted that this process is reversible. Under

electrochemically oxidizing conditions, the thiolates reassemble and the SAM can be easily regenerated.[26]

1.4 Implementing a new use of SAMs

SAMs are characterized by many qualities, as expressed in the previous paragraphs, and one of their possible future applications is in molecular electronics in substitution of traditional semiconducting components. Nowadays normal semiconducting electronic components are made up of layers combining metals like Ga, Zn, and semimetals like As, Te, deposited together. Until now less work has been carried out on structures in which an organic moiety was sandwiched between the basis substrate and the contact on top,[27,28,29] mostly for investigating electron transfer through molecules and its change by functional tail groups.[30] These studies are also of interest for electrochemical applications of SAMs as they can be exploited for the control of charge transfer in electrochemical reactions at interfaces. One example is the electrodeposition of metal on top of a SAM which results in a metal/SAM/metal hybrid system. To achieve this the tail group of the SAM molecules has to be properly tailored. Exploiting coordination chemistry by using, for example, pyridine as a tail group metal ions such as Pd^{2+} or Pt^{2+} can be coordinated and subsequently reduced to the metal as illustrated in Figure 4.[31] This scheme is of interest for molecular electronics as it allows the generation of not only metal/SAM/metal hybrid structures. Furthermore, it enables the deposition of metal clusters of a size which results in a Coulomb blockade[32] and a stepwise change in current which may have, in further developments, useful applications for a new generation of electronic components.

Alkane chains are rather poor conductors of electricity, so why bother about the use of aliphatic SAMs? They have served as model systems to understand charge transfer at the molecular level but for advanced applications their dielectric properties are of interest as they can improve the performance of gate oxide layers in transistors.[33] In hybrid metal-SAM systems where electronic functionality of molecules is envisaged, aromatic thiols are more interesting as their conductivity is well above the conductivity of chains consisting of methylene units. Considering the variability of SAM molecules the implementation of SAMs for organic-

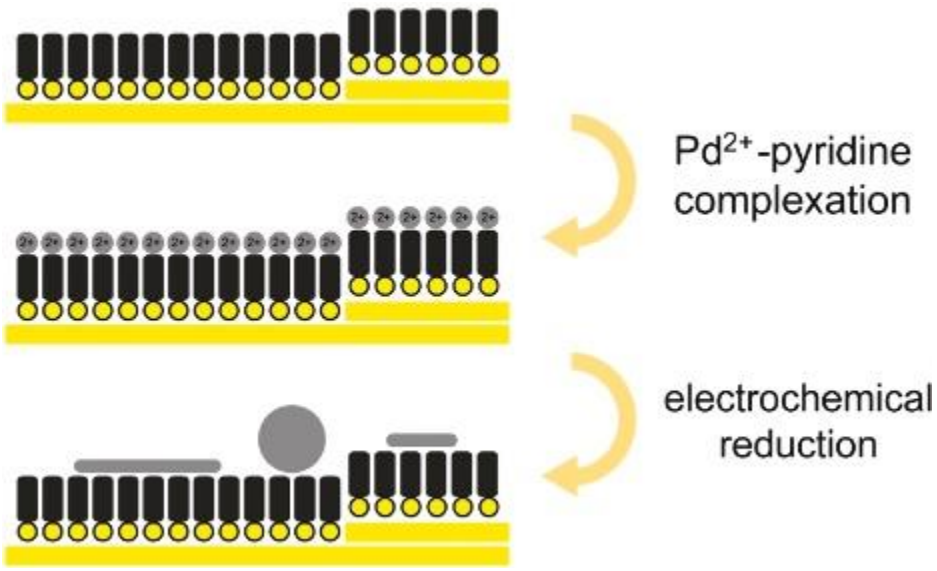

Figure 4: Scheme to illustrate the multistep process in which Pd nanoparticles are generated on top of a thiol SAM. Figure adapted from reference 31.

inorganic hybrid sandwich-like structures open up interesting opportunities for electronic components.

The aim of this research work is to control the various steps that ultimately allow the construction of a system, composed of a SAM with a metal layer or metal nanoparticles on top, and to characterize the systems by electrochemical means. The procedure consists in preparing the SAM outside an electrochemical cell followed by a transfer into the cell where further reactions take place. This way a Au substrate covered by a SAM can be electrochemically manipulated. If the terminal part of the thiol is functionalized to coordinate metal ions on top of the SAM, an electrochemical discharge triggers the formation of a metal layer or nanoparticles, depending on the details of the deposition process.[31,34,35] If the metal ions present in the electrolyte and coordinated to the SAM are different also alloy nanoparticles can be created which might be of interest considering the catalytic properties of alloy nanoparticles: for example, it is has been demonstrated that Ag nanoparticles encapsulated in an alloy Ag/Pd shell exhibit higher catalytic activity towards oxidation of formic acid in comparison with pure Pd nanoparticles.[36] The approach to be used in this research work is to study the deposition procedure step by step, by characterizing it by cyclic voltammetry to see if results add up with theoretical models. Only when there is confidence in the realizability of that step, the action moves on to the successive step, until the procedure is complete.

2 Characterisation Techniques

The samples prepared in this research work are analysed by electrochemical means. In additions to this macroscopic characterisation microscopic techniques are applied. Voltammetry and chronoamperometry belong to the first type, SEM (Scanning Electron Microscope) and AFM (Atomic Force Microscope) to the second one.

2.1 Voltammetry

Voltammetry is one of the most common techniques in electrochemical analysis. The basic tenet is to record the current while sweeping the potential in a defined way. For a heterogeneous electrochemical reaction, that is a reaction happening at the interface between a solid electrode surface and a liquid solution, two types of processes have to be considered: charge transfer and mass transport. The charge transfer step consists of electron transfer between the electrode and the electroactive species near its surface. Transfer of a single electron does not always result in a stable chemical species stable (for example, Fe^{2+} and Fe^{0} are stable species, but the intermediate Fe^{1+} is not), so several electron transfer steps might be needed. In addition to the charge transfer other chemical reactions can occur like addition of a ligand to a metal ion or molecular rearrangements. The mass transport processes are diffusion and convection through which the chemical species are transported to the surface of the electrode from the bulk of the solution and away from the surface of the electrode into the bulk of the solution. Considering the kinetics of an electrochemical reaction the bottleneck rule holds, that is, the slowest step determines the rate of the overall reaction. When the conditions in the system change, the rate determining step is affected. For example, the electron transfer step can become faster if the potential applied to the electrode is increased, because a higher potential increases the driving

force for the reaction. However, one has to keep in mind that, in some cases, a higher potential can also cause unwanted side-reactions that are difficult to control or that lead to undesired by-products. Moreover, when the electron transfer is fast, the rate might be controlled by diffusion. This mass transport limitation can be overcome to some extent by introducing convection by using either a rotating electrode or a stirrer inside the solution, even though the latter leads to less reproducible results. In both cases moving the liquid increases the rate at which species are transported to and away from the electrode.

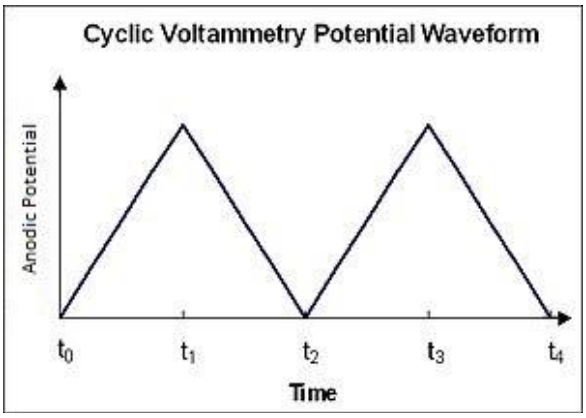

Figure 5: Example of voltage vs time ramp in cyclic voltammetry. Modified from reference 37.

To obtain information about electrochemical reactions one can record the current during voltammetric cycles. After a ramp of, say, positive going potentials (anodic sweep), there is a ramp of negative going potentials (cathodic sweep), to recreate conditions similar to the ones at the beginning of the cycle. This type of analysis is very common in electrochemistry, and is called "cyclic voltammetry". In the most common type of ramp a constant scan rate is applied, that is the voltage varies linearly with time as shown in Figure 5.[37] Depending on the type of voltammetric analysis other kinds of ramps are also applied.[38] With typical values for the scan rate on the order of tens of mV voltammetry takes at most a few minutes to be run. A typical cyclic voltammogram is shown in Figure 7[39]. From the shape of the I-V curves and positions of oxidation and reduction peaks information is extracted about the system. An important example is the Randles-Sevcik equation[40]

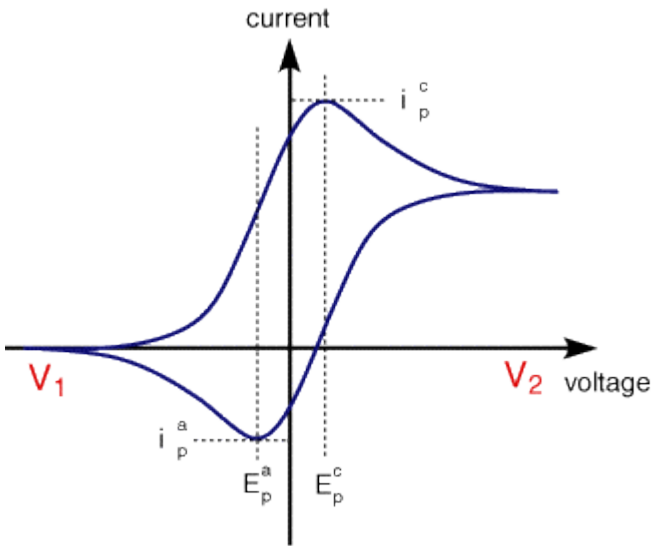

Figure 6: Example of i versus V voltammetric graph, that may result from the voltage ramps displayed in Figure 5.

$$i_p = 0.4463 n_e FAC \sqrt{\frac{n_e F v D}{RT}} \quad (1)$$

where i_p is the peak current, n_e is the number of electrons exchanged in the reaction, F is Faraday's constant, A is the area of the electrode, C is the concentration of the redox active species (expressed in mol/cm^3 and not in mol/l because other parameters are expressed in cm^3 and not in l), v is the scan rate, D is the diffusion coefficient, R is the universal gas constant and T is the temperature. The diffusion constant can be determined by measuring the peak current i_p as a function of the scan rate.

It is important to be reminded that this equation holds only when the rate determining step is controlled by charge transfer, and not by diffusion process. It should be noticed also that cycles

successive to the first one are not perfectly equal to this one, because a reverse voltammetric ramp does not exactly set the system back to the initial conditions; in other words, it shows a hysteresis that is more or less pronounced depending on the components under analysis.

2.2 Chronoamperometry

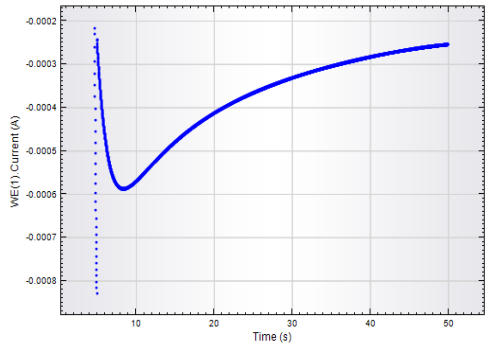

Figure 7: Example of current-vs-time chronoamperometric graph of a Au/Si substrate covered by DL-97 and immersed in 100 µM $PdSO_4$ solution that undergoes a nucleation step at -0.3 V for 0.1 s with an interval time of 0.0025 s followed by a growth step at -0.15 V for 45 s with an interval time of 0.01 s in electrolyte 10 mM $CuSO_4$ with Cu reference electrode. Different stages are easy to be spotted.

Chronoamperometry is a technique different from voltammetry. While in voltammetry the current is recorded as a function of the potential, in chronoamperometry the potential is set to a value and the current is monitored as a function of time. It is noted that while recording an i-t curve different values of the potential can be applied for different periods of time. A typical chronoamperometric curve is displayed in Figure 7, while Figure 8 shows its corresponding potential-time graph, in which the different potential steps are clearly seen. The kind of information that can be derived from chronoamperometry is different from voltammetry. For example, from the shape of the i-t curve one can obtain information about nucleation and growth processes. Moreover, because the product of current and time is charge, the amount involved in a redox reaction can be calculated from the integral of a chronoamperometric curve taking into account that the amount of a substance consumed is proportional to the charge according to Faraday's law.

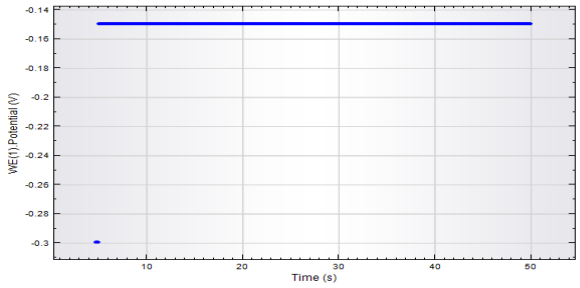

Figure 8: Potential-vs-time graph of the same scan as in Figure 7. The different steps at which potential is constant are easy to be spotted.

Modern instrumentation allows the determination of the charge by numerical integration of the curves which then allows a straightforward calculation of the thickness h of a layer deposited onto an electrode according to

$$h = \frac{q \cdot AW}{n_e \cdot F \cdot \rho \cdot A} \qquad (2)$$

which contains the number of electrons involved (n_e), the atomic weight of the metal (AW), its density (ρ) and the total charge passed through the electrode (q). It is important to remind that this equation holds in this form only when current efficiency is 100%; otherwise, a corrective term needs to be introduced.

Figure 9: Image of an SEM apparatus. The microscopy chamber on which the electron column sits is seen on the left.

2.3 Scanning Electron Microscopy (SEM)

SEM (Figure 9[41] shows an example of such a system) is an essential tool to inspect samples when a higher magnification is required than what is achievable with optical microscopy.

SEM uses electrons instead of light as a mean to examine the surface. Because the wavelength of an electron at voltages typically used in SEM (ranging between fractions of kV and beyond 10 kV[42]) is on the order of Å according to the following formula[43]

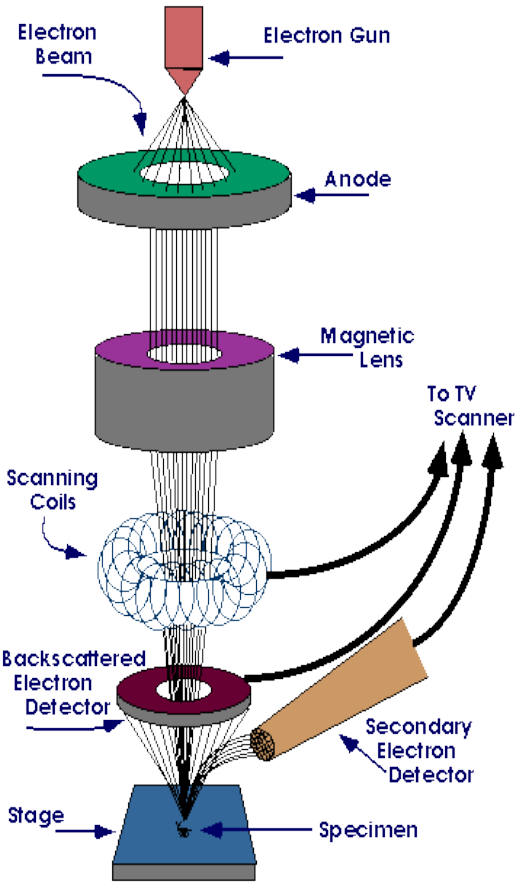

Figure 10: Scheme of the setup of an SEM showing how the various parts work and are arranged inside the chamber. For further details, see text.

$$\lambda = \frac{h}{\sqrt[2]{2 \cdot m \cdot KE}} \qquad (3)$$

i.e., the diffraction limit which determines the maximal resolution in microscopy is at much smaller dimensions for electrons compared to visible light. In Equation 3 λ is the wavelength associated to the electron, h is Planck's constant, m is the mass of the electron and KE its kinetic energy.

In the SEM apparatus (Figure 10[44] displays a scheme of how the various parts are arranged inside the chamber of the apparatus), a gun emits electrons through various mechanisms: it may be a W piece that, by being heated at around 3000 °C, gives off electrons (thermionic emission), or a LaB_6 filament that works on an analogue principle. The former has to be replaced more often because of evaporation, while the latter needs better vacuum even though it is able to operate at lower temperature. There is a third option, the field emission mechanism: it concerns electron extraction from a filament by applying a sufficiently high electric field, sometimes assisted by an elevated temperature. The emitted electrons pass through a series of apertures and deflection coils (magnetic lenses) whose purpose is to narrow and collimate the electron beam on the target to be analysed, so that it is in focus. The stage on which the sample sits can be moved either vertically, to provide a further way to adjust to the focal length, or laterally, to allow the instrument to acquire a map of the whole sample. The chamber in which the electrons

fly and the sample is set requires high vacuum because if atoms were present in it, they would hamper the flight of the electrons, reducing their mean free path.

SEM relies on the interaction of the electron beam with the substrate under analysis. Essentially, the electrons of the primary beam penetrate the sample and interact with the electrons of the sample (that is, they exchange energy with them). At this point, secondary electrons and backscattered electrons can arise. Secondary electrons involve inelastic scattering with the electrons of the sample, and the difference in the electron energy is characteristic of the material of the sample, from which elemental composition can be drawn. Backscattered electrons instead involve elastic scattering with the electrons of the substrate surface, and no elemental information can be achieved about the sample. The detector scans the surface point by point thus creating a detailed map of the surface. An example of an SEM image is displayed in Figure 11.

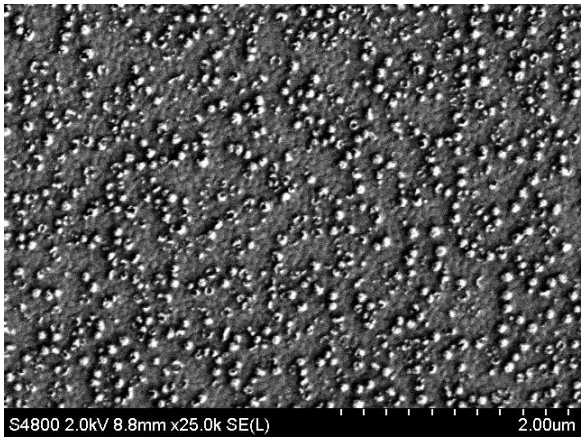

Figure 11: Example of an SEM image of the surface of a substrate covered by the organic molecule DL-97 (detailed further down in the text) and mixed Cu-and-Pd nanoparticles. The resolution achievable with this technique can reach the dimensions of the nanoparticles themselves.

2.4 Atomic Force Microscopy (AFM)

AFM (an apparatus of this kind is exemplified in Figure 12[45]) is a very powerful tool to gain a detailed image of a surface at the nanometric scale. In comparison with STM (Scanning Tunnelling Microscope) or SEM, it does not function on electrons used as a beam, instead it functions on mechanical forces. Like STM it does not require vacuum and can work even in a liquid environment.

A cantilever (generally made of Si or Si_3N_4) is connected to a piezoelectric device and, at the terminal part, it has a tiny tip pointing downwards; the dimension of the cantilever is on the order of tens of µm and the tip has a typical radius of curvature of a few nanometres. When this tip is put in contact with the substrate surface to be

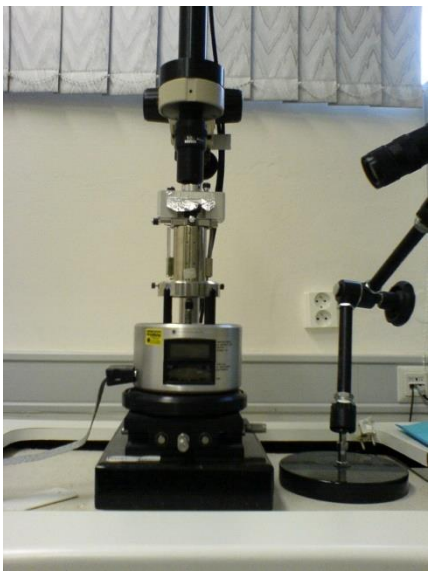

Figure 12: Example of AFM apparatus. The sample is put in the chamber, at half of the height of the apparatus.

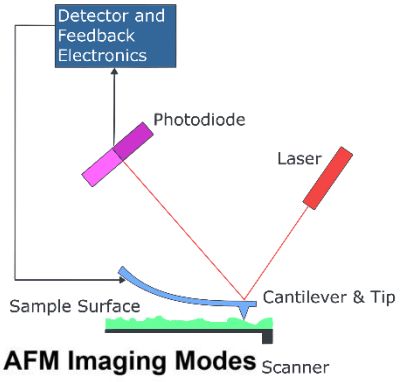

Figure 14: AFM Modes of use, contact mode (normal dragging over the surface) and tapping mode (the tip is oscillated while being dragged).

analysed, the piezoelectric device moves the tip line by line across the surface (the X-Y-plane). Also the Z-position of the tip is adjusted through the piezoelectric device.

Scanning the tip across the surface any topographical change will bend the cantilever in an elastic way, following Hooke's law. The bending is detected by a laser beam which is reflected from the end of the cantilever as illustrated in Figure 14.[46] According to the bending of the cantilever, it will be reflected in different directions and a position sensitive photodiode collects the light of the reflected laser beam. The changes in position is translated into a height information by the computer and fed back to the Z-control. In a nutshell, this type of microscopy does not "see" the surface, it instead touches it and by following the height profile generates a map of the surface. This technique does not require the sample to be coated, so its preparation does not involve steps that would alter it.

There are three main modes of use of AFM, namely contact mode, tapping mode and non-contact mode. The contact mode, displayed in the upper part of Figure 14,[47] works essentially as already expressed above, that is, by simply dragging the cantilever across the surface. Despite being the classical use of AFM, it is preferentially used on sufficiently stiff surfaces, because pliable surfaces may be scratched and damaged by the scanning tip. Also, nano-objects that are not strongly adhering to the surface may be even displaced.[48] Tapping mode, displayed in the lower part of Figure 14[47] which was specifically devised for soft samples. It works by eliciting controlled vertical oscillations while the tip moves across the surface. The contact with the surface and, thus, the topography is sensed by a change in the frequency of the oscillation. Since the forces on the surface can be smaller than in the contact mode a precise mapping is possible without damage and the problem of dislocating loosely bound nano-objects is significantly reduced. Non-contact mode consists in oscillating the cantilever at a short distance from the sample, whose surface will interact through van der Waals forces, thus affecting the position of the cantilever; from this alteration, the topography of the sample can be worked out easily. This imaging mode is used in a similar manner to the tapping mode, that is, when it needs to avoid damage on the sample surface, but it owns another characteristic that makes it useful: if

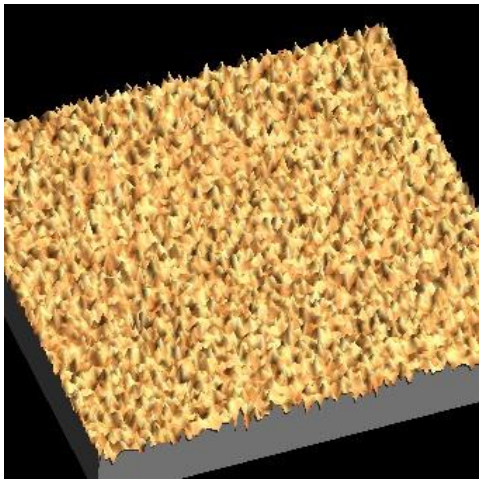

Figure 15: AFM image of the surface of a sample covered by DL-97 and mixed Cu-and-Pd nanoparticles obtained by electrochemical deposition. In the image the uniform grainy surface is easy to be seen.

above the surface there is some fluid, an AFM working in non-contact mode will sense both it and the surface.[49]

To visualise and process AFM data various programs can be used, like Callisto[50] or Gwyddion,[51] but in this research work WSxM,[52] which can read data from different types of probe microscopy, has been used. Figure 15 shows a surface image that can be attained with this type of program. To be noticed is that, also with this type of microscopy, the resolution of the nanometric map depends on the speed with which the cantilever passes over the surface: if it is too fast, the apparatus may lose some details. The more evident asperities a surface has, the more slowly the tip will have to screen the surface.

The tip may be modified if special needs arise: for example, a protein-coated tip specifically interacts with high selectivity with determined biochemical species on the surface,[53] a graphene-coated tip shows low tip-sample interactions and a longer life time of the tip itself,[54] a diamond tip is used if exceptional resistance to wear is required.[55]

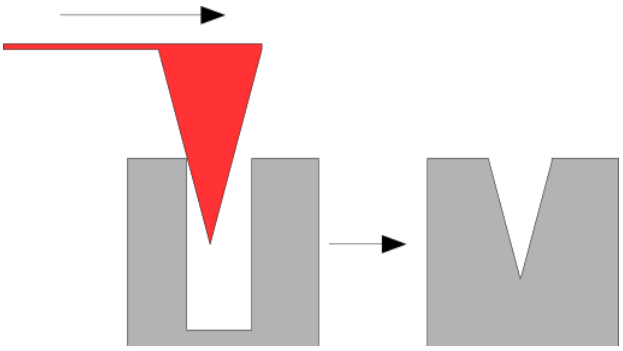

Figure 16: Example of how the image of a vertical wall is distorted by the shape of an AFM tip.

While AFM offers the advantage of a relative operational simplicity, one has to bear some limitations in mind which are intrinsic to the way data are acquired: if the surface has vertical walls, recesses or mushroom-like protrusions, the cantilever will still feel them, but, because of the convexity of the tip, on the map it will result in an artifact like the one depicted in Figure 16.[56] Similarly, if the tip, because of wear and tear, has become blunt, it will lose details of nano-objects with a small curvature radius. However, under favourable conditions a state of the art AFM operating in ambient can achieve a vertical resolution of 0.01 nm and a lateral resolution of better than 0.5 nm.[57]

3 Experimental methods

3.1 Sample Preparation

The substrates used for the experiments consist of Au substrates of roughly squared shape and an area of about 1 cm^2. The substrates are cut from a 4 inch wafer of a 100 nm Au film evaporated onto Si with a 5 nm Ti interlayer as adhesion promoter. The wafers are purchased from Georg Albert PVD Beschichtungen. Until used they are stored in a vacuum chamber to prevent them from being contaminated.

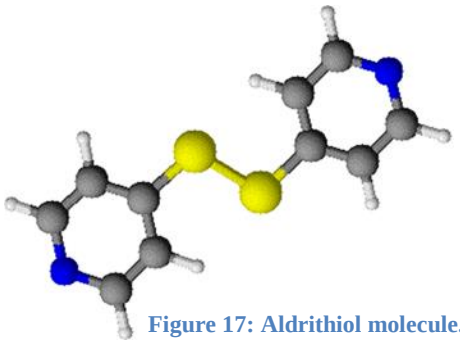

Figure 17: Aldrithiol molecule.

The aldrithiol layer preparation solution is made up of 1 mM aldrithiol (shown in Figure 17) in ethanol with a fraction of grain of KOH so that the pH~11. Aldrithiol comes from Sigma-Aldrich and has a purity of 98%, ethanol comes from AnalaR NORMAPUR and its purity is 99.9%. KOH comes from Fluka (titration value > 86%), Na less than 0.05%.

1 mM $CuSO_4$ solution is prepared from $CuSO_4 \cdot 5H_2O$ (Sigma-Aldrich, 99.999% pure with trace of metal basis) and sulfuric acid to attain pH~1. The sulfuric acid comes from Sigma-Aldrich and its purity is 99.999%.

100 µM $PdSO_4$ solution is prepared from $PdSO_4$ (Sigma-Aldrich, purity 98%) and adjusted with sulfuric acid to pH ~1.

For the solutions ultrapure water from a Millipore system was used with a specific resistivity of 18.2 MΩ·cm at 25 °C.

An aldrithiol layer is prepared by immersing a Au/Si sample in a vial with such a quantity of aldrithiol solution that the sample is submerged wholly. After overnight immersion (~15 h), the substrate is extracted, rinsed with ethanol and blown dry with a nitrogen stream. For the characterisation of the just prepared aldrithiol SAM the sample is mounted in the electrochemical cell and a voltammetric analysis is performed in 0.1 M aqueous KOH to avoid protonation of split aldrithiol. The scan is run from 0 V to -1.1 V against a Pt reference electrode with a scan speed of 0.01 V/s.

The experiment to check the behaviour of an unmodified aldrithiol layer towards Cu deposition involves overnight immersion of the sample in aldrithiol solution, then the sample is rinsed with ethanol, blown dry with nitrogen flux, mounted in the electrochemical cell and using 1 mM $CuSO_4$ solution in H_2SO_4. Scans are run from 0 V to -0.8 V against a Cu reference electrode. Scan speed is 0.02 V/s

Experiments to check the behaviour of aldrithiol layers modified by coordination of Pd on top of the SAM are performed in two different ways. After the usual formation of the aldrithiol layer by overnight immersion in 1 mM aldrithiol in ethanol solution, the first one is an immersion in another vial full of 100 µM $PdSO_4$ solution in acidic environment (H_2SO_4) for not longer than 10 minutes. Then the substrate is rinsed, blown dry again, mounted in the cell and the voltammogramme is run using 0.1 M sulfuric acid. The other route is to mount the sample in the cell without exposure to the $PdSO_4$ solution, but instead this electrolyte is directly filled into the cell, and then a voltammetric scan is run between 0.2 V and -0.8 V against a Pt reference electrode with a scan speed of 0.02 V/s.

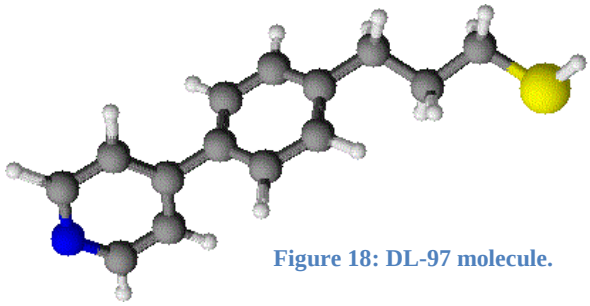

Figure 18: DL-97 molecule.

The other type of SAM investigated consists of 3-(4-pyridine-4-ylphenyl)propane-1-thiol, shown in Figure 18 and called for ease DL-97. The synthesis of DL-97 has been reported previously.[58] The experiments with DL-97 are fully analogous to the experiments with aldrithiol.

The solution for preparing DL-97 SAMs is made up of 100 µM DL-97 in ethanol with a fraction of a grain of KOH to achieve a basic pH. The solution needs alkaline environment because top nitrogen should not be protonated, but, if it is too basic, hydroxyl ions can compete to some extent with DL-97 in occupying available sites on the substrate, leading to poor film quality. Introduction of a more mildly alkaline solution (pH~8) solves the problem. $PdSO_4$ solution used in the experiments with DL-97 is 100 µM.

In addition to Au/Si substrates, Au/mica substrates are used in selected experiments. They are also purchased from Georg Albert PVD Beschichtungen and stored in a vacuum chamber. After cutting to size the substrates are flame-annealed uniformly for ~20 s before the deposition of DL-97 in the preparation vial.

The electrolytes ($PdSO_4$, $CuSO_4$, sulfuric acid) used in experiments related to DL-97 are the same as for experiments with aldrithiol.

For the experiments assessing the Cu deposition on DL-97 coated substrates a sample is taken out of a normal preparation vial, rinsed with ethanol and blown dry with a nitrogen stream. After mounting it in the cell as usual and filling in a 1 mM $CuSO_4$ solution, voltammetric scans are performed either without wait time between scans or with wait time whose length is varied between 6 and 18 minutes. Scans are run from 0 V to -0.75 V against Cu reference electrode at a scan speed of 0.01 V/s.

The experiment to assess the behaviour of Pd on DL-97 layer is fully analogous to the one described above, but $CuSO_4$ solution is replaced by $PdSO_4$ solution and there is no wait time. Scan is run from 0 V to slightly more than -0.95 V against Pt reference electrode. Scan speed is 0.01 V/s

The experiment with mixed Cu-and-Pd nanoparticles above DL-97 layer is based on Au/Si substrates on which DL-97 is deposited from a solution of the thiol in a preparation vial, followed by Pd adsorption on top in the incubation vial full of $PdSO_4$ solution, analogously to what is described in the preceding paragraph with aldrithiol. Then the substrate is rinsed with ethanol, blown dry with N_2 stream and mounted in the electrochemical cell. As electrolyte 1 mM $CuSO_4$ is used. Scans are run from 0 V to -0.8 V against Pt reference electrode with the usual scan speed of 0.01 V/s.

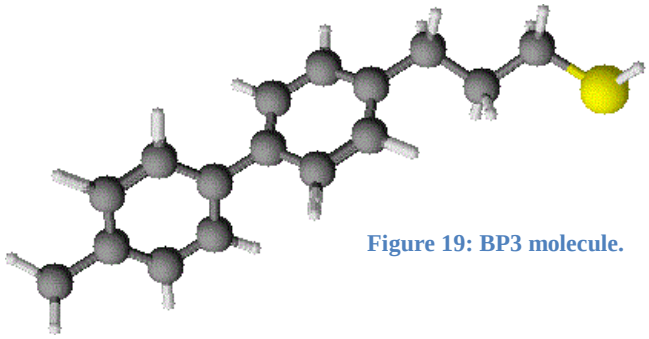

Figure 19: BP3 molecule.

For testing to what extent metal penetrates the SAM (more details in section 4.2.4) another molecule is introduced, 3-(4'-methylbiphenyl-4-yl)propane-1-thiol, called for simplicity BP3 (shown in Figure 19). A BP3 solution is made up of 100 µM BP3 molecule in ethanol with no pH adjustment. The BP3 synthesis has been reported previously.[59]

For the control experiments with BP3 SAMs a normal Au/Si substrate is immersed for 2 hours in a vial full of 100 µM BP3 solution. Then, the sample is taken out of the solution, rinsed with ethanol, blown dry with nitrogen stream and mounted in the electrochemical cell. The experiment is performed in a 100 µM $PdSO_4$ solution to assess the extent of penetration of Pd into the SAM. The scans are run from 0 V to -0.95 V against Pt reference electrode. Scan speed is 0.01 V/s

In the experiment to assess the influence of sulfuric acid on the layer, the procedure follows the same guidelines explained for the already described experiment but the cell is filled with 0.1 M sulfuric acid only. The scan are run from 0 V to -0.95 V against Pt reference electrode. Scan speed is 0.01 V/s

The experiments of selective deposition are performed on the usual Au/Si substrates on which DL-97 is deposited overnight from the 100 µM solution in ethanol already described above. They are then removed from the solution, rinsed with plenty of ethanol, blown dry with nitrogen stream and mounted on a vertical clamp held by a heavy stand (description in section 3.2.1). To let Pd ions selectively deposit on the various substrates, they are half-dipped in it for no longer than 10 minutes. Then, they are rinsed, blown dry again and mounted in the electrochemical cell. Not only voltammetric experiments but also chronoamperometric experiments were performed. The chronoamperometric procedure is composed of two parts: the first one is a short nucleation step at negative potentials, during which nucleation is triggered, the second one is a long growth step at less negative potentials. In searching for the ideal time pattern for the best deposition, several combinations have been tested: for the nucleation step, voltage varies between -0.4 V and -0.25 V, and time varies between 0.5 s and 0.01 s; for the growth step, voltage is always -0.15 V, and time varies between 65 s and 30 s. The interval time, that is, the shortest time between two subsequent sampling points, varies between 0.01 s and 0.0025 s (it defines the density of points in the graph). Both potentials are registered against Cu reference electrode. In these experiments the electrolyte is always an acidic aqueous 10 mM $CuSO_4$ solution.

3.2 Deposition

3.2.1 Electrochemical Setup

The cell consists of a standard three electrode setup with the SAM coated substrate as working electrode, a counter electrode and a reference electrode. An image of the fully mounted cell is shown in Figure 20 and a schematic drawing of the fully mounted cell is displayed in Figure 21. The main cell consisting of a KEL-F cylinder with a central hole of approximately 8 mm in diameter is fixed to a support stand by screws. The substrate is attached to the bottom of the cell using an O-ring as watertight connector.

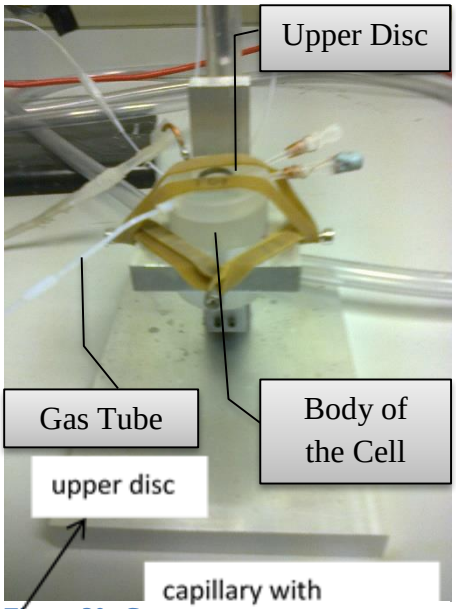

Figure 20: Cy… y mounted.

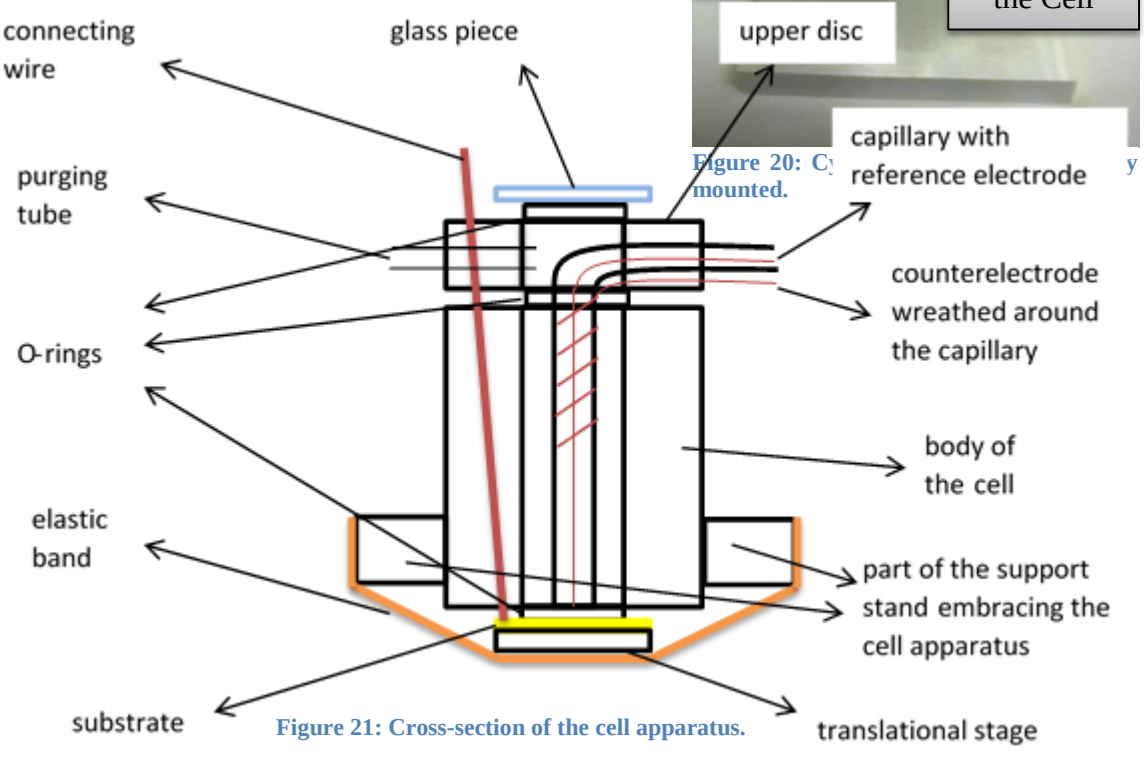

Figure 21: Cross-section of the cell apparatus.

The counter electrode and the reference electrode are mounted on a KEL-F disk which is placed on top of the main cell. It also contains a port for attaching a tube to purge the cell with nitrogen. The contact with the working electrode is made of a wire which is inserted through the cell wall and touches the upper part of the substrate out of the O-ring with without scratching it, to warrant the circuit to be closed. The translational stage (the small platform under the cell on which the substrate is set) is pushed upwards by a spring mechanism, so that the O-rings warrant the system to be leaktight and the wire is in constant contact with the substrate surface. All this structure is put on a support stand and is held together by an elastic band with sufficient force to ensure that the system is leaktight. Between the cylinder and the disc there is an O-ring and, around it, a wider, thinner O-ring avoids electrolyte spillage by stopping liquid from

spreading beyond it. In the disc there are three outlets: the first one is for the capillary that contains the reference electrode, the second one is for the counter electrode, that is wreathed around the capillary but does not get too low, so that interference with the reference electrode is minimized, and the third one is an inlet for purging gas, to obtain a protected atmosphere inside the cell. A Teflon tube connected to a N_2 line is fitted to the inlet. The reference electrode is mounted in a Luggin capillary very close to the surface of the working electrode in order to allow an accurate setting of working electrode potential. For simplicity, depending on the experiment, Pt or Cu are used as reference electrodes. They provide sufficiently stable potentials as electrolyte concentrations are not significantly changed during the electrochemical experiments. The potential of the working electrode is sensed relative to the reference electrode and set or corrected by the instrument depending on the procedure applied.

Figure 22: AUTOLAB 83554 instrument.

Above the disc, another O-ring connects it to a glass piece to grant the cell being almost airtight; almost, because gasses in it have to exit somewhere, so this set-up is a trade-off between airtightness and need to release gases from inside.

All experiments are performed with the use of the computer program NOVA 1.10 connected to an AUTOLAB 83554 potentiostat (Figure 22) which in turn is connected to the cell by crocodile clips.

Before the cyclic voltammogram is run, the cell is purged with nitrogen for 30 minutes to eliminate features from O_2 appearing in the voltammogram itself. After the purging time, the tube is retracted but not removed from the inlet and the gas flow maintained in order. A detailed study about the ideal length of the purging time has not yet been carried out, but it has been observed that a purging time of around 30 minutes results in a sufficient reduction of oxygen.

Throughout the series of experiments the setup used for the layer penetration tests was slightly modified. While the body of the cell remained unchanged, two outlets out of three of the disc above it normally occupied by purging cable and reference capillary with reference electrode mounted in it are now blocked with Blu Tack adhesive. The port for the counter electrode is still present, but the counter electrode itself is shaped into a ring around the reference capillary without touching it directly. The cover glass is substituted by a cap in which a capillary with reference electrode wire is inserted. The capillary is fixed to the cap with a cyanoacrylate glue and a hole close to it serves as feedthrough for the purging cable. This setup is not completely airtight so gas being purged can escape from inside the cell. The correct distance of the reference electrode from the substrate is based on voltammograms with the Cu deposition peak least shifted to negative potentials serving as optimisation criterion. With this apparatus, there needs to be compromise between proximity of the reference electrode to the substrate surface, so that the measure is as accurate as possible, and effective quantity of electrolyte that reaches the reference electrode. Indeed, because the capillary in which it is set is very thin, if the flux through it is too low, the resultant measure can be biased. If the Cu reference electrode and a 1 mM $CuSO_4$ in H_2SO_4 solution as electrolyte are used, the peak should be around -0.1 V. Once the best position has been found, the Cu reference wire is fixed by bending around the capillary and wrapping it with scotch tape.

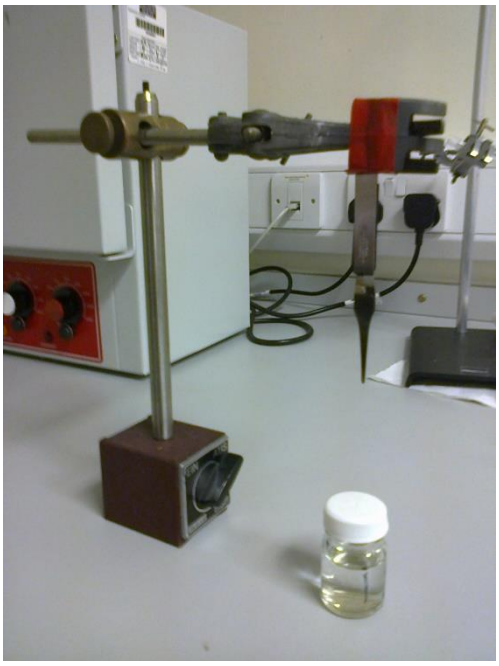

Figure 23: Apparatus aimed to half-dipping operation. The clamp can be moved up and down to partially immerse the sample in the incubation vial full of 100 µM $PdSO_4$ solution, located beneath the clamp itself.

The apparatus used for the half-dipping experiments for partial deposition is shown in Figure 23. It allows up-and-down movements of the sample above and into a vial and when the clamp is moved, it is dipped into the already described $PdSO_4$ solution. The electrode setup is different from the one used previously: the counter electrode is no longer ring-shaped, instead it is wreathed around the capillary. No purging was applied when using this cell.

3.2.2 Deposition Procedure

The purpose of running voltammograms is to test the electrochemical behaviour of the system in successive cycles and also to study its reproducibility over more cycles. The highest and the lowest potentials are chosen so that no unwanted side-reaction occurs, that could spoil the experiment. Therefore, especially the lowest potential has to be chosen with particular care, because reduction of H^+ ions to H_2 produces bubbles that severely affects the voltammogram. This limit has to be chosen according to the reference electrode, because Pt and Cu have different potentials with the same electrochemical system. The number of cycles is mostly capped to two or three per experiment and they are analysed by plotting them at the same time on the computer so that it is easy to spot similarities among cycles or specific trends.

The experiments of selective deposition are performed by using chronoamperometry instead of voltammetry. The procedure consists of applying a series of different potentials. By varying potentials and duration, conclusions on the behaviour of the system can be inferred.

3.3 Characterisation

Samples obtained in the experiments of selective deposition are briefly analysed with an optical microscope to evaluate their morphology on the microscale. Only the samples that show the most uniform coverage are later analysed with SEM or AFM.

The SEM apparatus uses an acceleration voltage of 2000 V, no deceleration voltage, a working distance of 8.9 mm, an emission current around 10 µA for all the images taken, with high lens mode.

Analysis is performed also through the use of AFM. The images were collected on a Bruker Dimension Fast Scan system in tapping mode with a Veeco SNL-A cantilever whose tip is made of Si and whose elastic constant is 0.58 N/m.

4 Results and discussion

4.1 Experiments with aldrithiol

4.1.1 Characteristics of aldrithiol molecule

The plan for this research project is to test the various steps of the deposition procedure outlined in section 3.1 by cyclic voltammetry one by one, by performing them progressively, in order to establish the optimal conditions for the metal deposition. The molecule used as basic building brick for the self-assembled monolayer is aldrithiol, a symmetrical disulfide that when it is exposed to a Au surface splits down into two equal moieties, becoming in fact a thiolate, as outlined in Figure 24, when forming an ordered SAM. The nitrogen on top of the split molecule, if it is deprotonated, can coordinate metal ions allowing them to be discharged

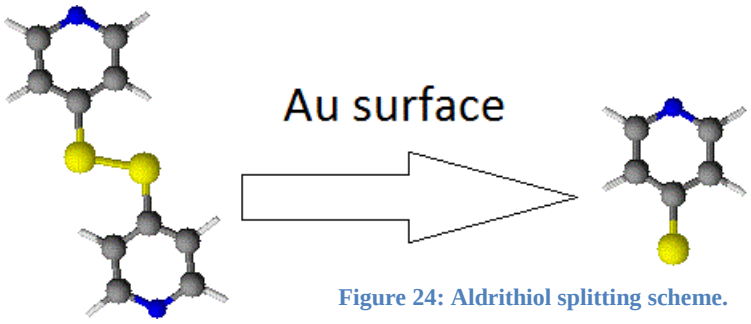

Figure 24: Aldrithiol splitting scheme.

in a well-controlled manner and turned into neutral metal atoms that compose a metal layer above the aldrithiol sublayer.

4.1.2 Aldrithiol layer stability test

The voltammograms of Figure 25 running from 0 V to -1.3 V, represent three consecutive cycles, of an aldrithiol SAM on Au/Si in KOH as electrolyte. A clear peak can be observed at about -1.0 V which indicates the reductive desorption of the thiol as known from the literature.[9] At this cathodic potential the mercaptopyridine is reduced, the thiolate is released and diffuses, away from Au surface into the bulk solution. It is better not to extend the voltammogram to excessively negative potentials, otherwise hydrogen evolution from breakage of water molecules takes place, thus, unpredictably affecting the voltammogram by random signals triggered by bubbles. The thiolate readsorption peaks can be spotted on the way back at a slightly less negative potential than the one of the first desorption peak, and this means that destruction of the SAM is at least partially reversible (partially because the desorption peaks in successive scans are smaller than in the first scan).[1] The reversibility is only partial because in the course of the experiment some side-reactions happen that spoil the nature of the system, leading to products whose behaviour does

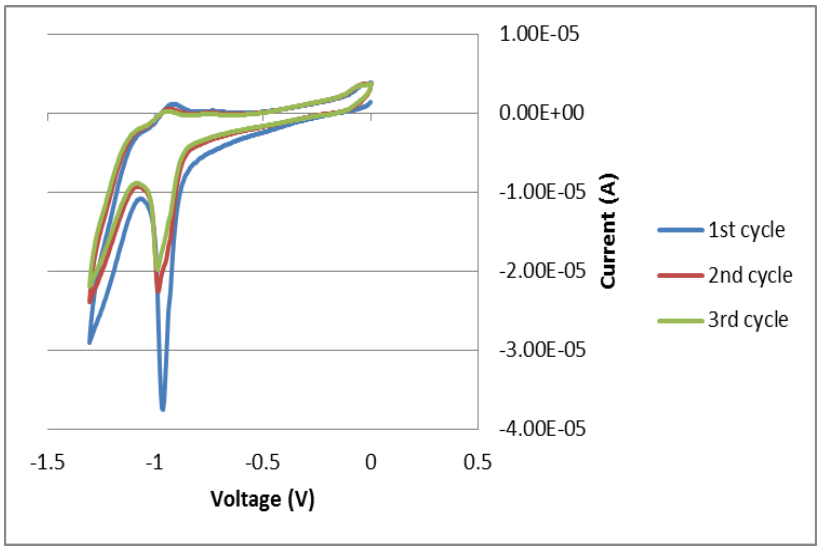

Figure 25: Cyclic voltammogram of an aldrithiol SAM on Au/Si substrate, in 1 M KOH as electrolyte and with the use of Pt reference electrode. 3 consecutive cycles of the same scan are run, that begin from 0 V and go towards negative potentials till -1.3 V.

not coincide with the one of aldrithiol. This desorption experiment establishes the overall stability range of the mercaptopyridine SAM.

4.1.3 Complexation of aldrithiol layer with Pd ions

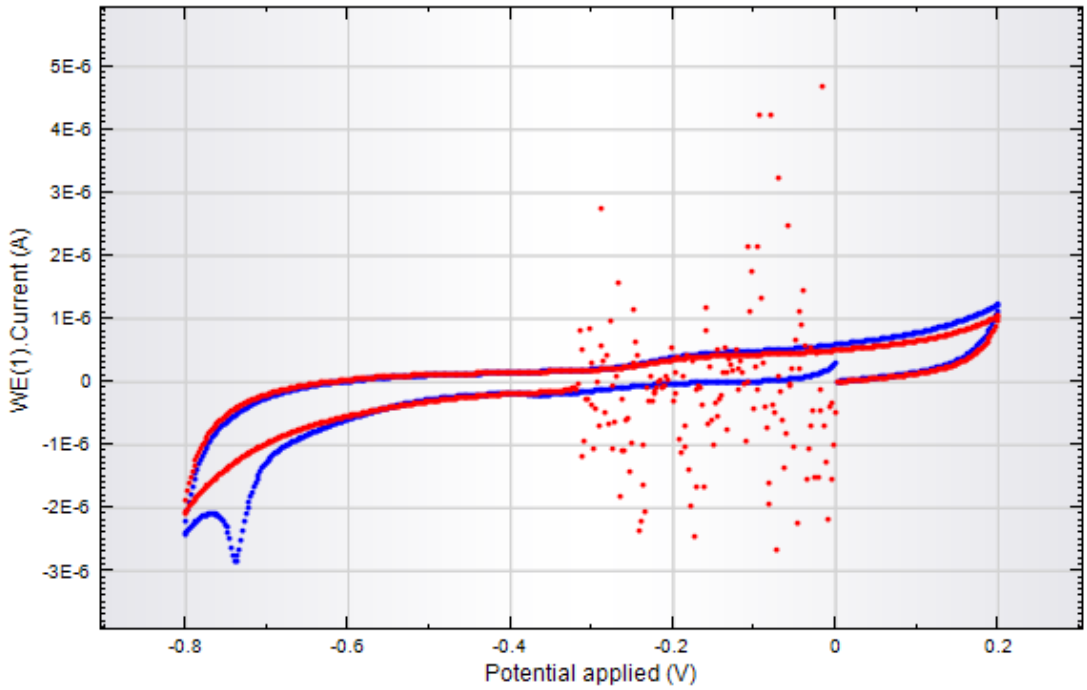

Figure 26: Cyclic voltammogram of aldrithiol SAM on Au/Si substrate with Pd added on top, in 0.1 M sulfuric acid as electrolyte and with the use of Pt reference electrode. Each cycle ranges between 0 V and -0.8 V and goes initially towards negative potentials. First cycle is blue, second cycle is red.

In the next step metal deposition onto an aldrithiol SAM modified electrode was tested. From the metals studied, Pd or Cu, the former was the first whose deposition was attempted. Figure 28 shows the first two voltammetric cycles of a sample in sulfuric acid as electrolyte. Following the scheme illustrated in Figure 4, the mercaptopyridine SAM had been exposed to the $PdSO_4$ solution prior to the electrochemical reduction of Pd on top of the SAM. As seen the reduction of Pd is irreversible,[9] since the sharp peak between -0.7 V and -0.8 V seen in the first scan is absent in the second one (at less negative potentials there is, for unknown reasons, a zone where the current fluctuates but does not affect the results as it is not in the potential range of interest).

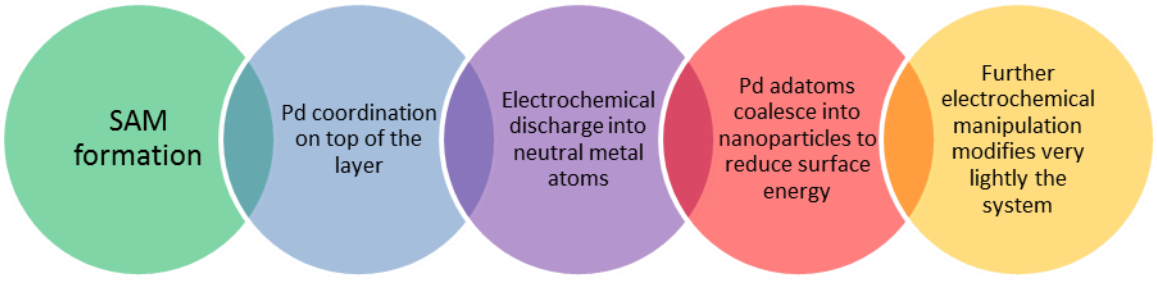

Figure 27: Nanoparticles evolution mechanism.

It has been suggested that nanoparticles formation is triggered, as it happens in experiments with the same molecules under similar conditions:[9] if further cycles were performed, neither desorption nor readsorption features would come out. This route to develop nanoparticles

above aldrithiol looks interesting, not only because of the particular way they are created, but also because, in general, nanoparticles themselves have demonstrated physical chemical properties of great relevance, and it may become very useful in the future. The proposed mechanism to explain the nanoparticle evolution on top of SAM is summarised in Figure 27. It is simply based on elementary steps established in surface science and electrochemistry.

4.1.4 Cu deposition from solution on aldrithiol layer

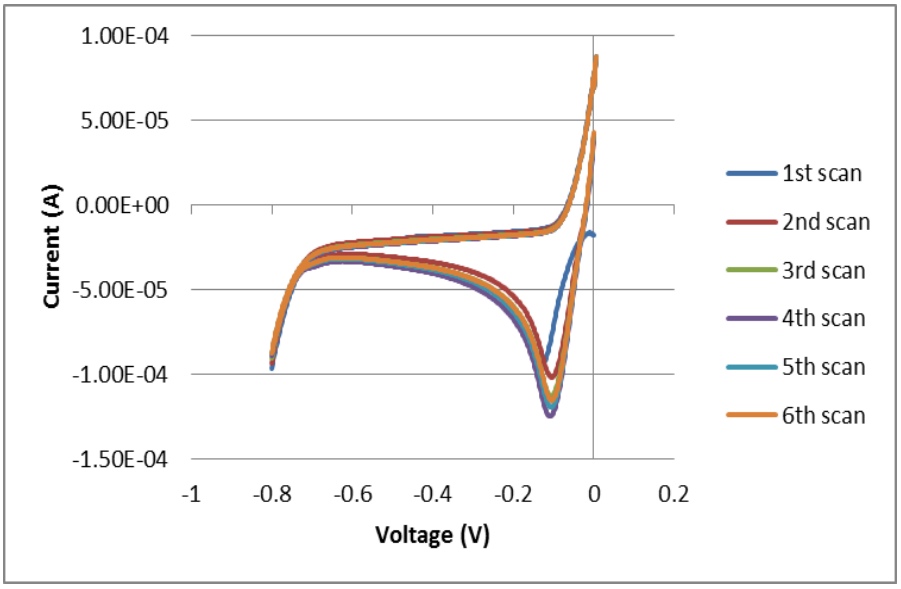

Figure 28: Cyclic voltammogramme of Cu deposition from 1 mM electrolyte $CuSO_4$ on aldrithiol SAM with Cu reference electrode. 6 scans are run, whose only the first cycles are shown, that begin from 0 V and go to negative potentials till -0.8 V. Between a scan and the successive one a time variable between 6 and 8 minutes is awaited.

Cu was tested, too, and its deposition on top of an aldrithiol SAM shows a very interesting behaviour. If there is a waiting time between two successive scans, the current increases with each scan. However, if there is no waiting time, the current is lower. This dependence is only observed for Cu but not for Pd (however, the comparison is not completely correct since the solutions in cell differ also in the rest of the chemical composition). An example of this behaviour is exemplified in Figure 28. This behaviour is quite particular, and for the moment no explanation exists to clarify it. Unfortunately, a suspicion arises: because in Cu deposition experiments peaks are located at very low potentials, it may be that some Cu atoms (and similarly, also Pd atoms in other experiments) get intermingled inside the aldrithiol layer. The following simple electrochemical inference easily explains the phenomenon: if a metal ion is in direct contact with the electrode surface, the resistance is so low that even at potentials slightly below 0 V it will be reduced. Conversely, if the organic layer is put in between the ion and the electrode surface, the resistance will be much stronger and more negative potentials will be necessary to reduce the ion. This inference pushes to suspect about peaks too close to 0 V because perhaps some ions can slip under the organic layer. This theory is underpinned by the fact that the split aldrithiol molecule is stiff but quite short, so it might be penetrable to some extent. A control experiment with Cu ions from electrolyte that are reduced at the bare Au substrate surface show features similar to those seen

in experiments on aldrithiol modified substrates. This confirms the suspicion, and puts the research on the way to develop a different molecule that is less penetrable to ions.

4.2 Experiments with DL-97

4.2.1 Characteristics of DL-97 molecule

The molecule investigated in the following is outlined in Figure 18. It is considerably longer than aldrithiol, with which it has in common the thiol head and the pyridine tail. In between there are a propyl chain and a benzene ring. The interactions between adjacent molecules of DL-97 are stronger compared to aldrithiol because there are an additional aromatic ring and a short hydrocarbon chain which improves the overall robustness and, thus, renders the layer more stable than the one composed of aldrithiol. The fact the film is thicker and its overall molecular packing is better should prevent ions from penetrating the SAM.

4.2.2 Behaviour of Cu on DL-97 layer

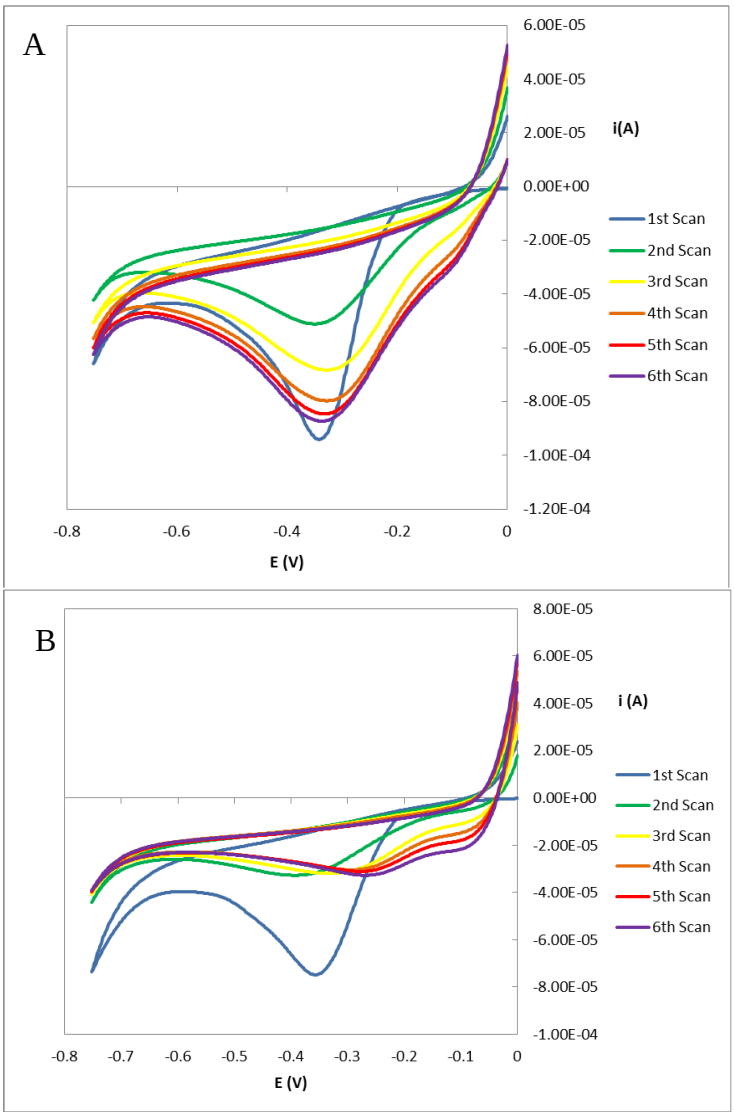

Figure 29: Cyclic voltammograms of Cu deposition on DL-97 using an acidic 1 mM $CuSO_4$ electrolyte and a Cu reference electrode. 6 scans were recorded with each scan comprising 6 consecutive cyclic voltammograms. For clarity only the 1st cyclic voltammogram of each scan is shown with the potential starting at 0 V and reversing at -0.75 V at a scan rate of 20 mV/s. In graph A the scans are separated by a waiting time between 6 and 18 minutes at open circuit potential, graph B shows scans without any waiting time.

The first thing to be verified is whether Pd and Cu deposition shows a molecule dependent behaviour, that is, a difference between DL-97 SAMs and aldrithiol SAMs. Cu deposition is tested in an experiment equivalent to the one with aldrithiol (section 4.1). Figure 29 shows two different experiments which differ in the time between two successive scans. If there is a waiting time between them the current registered for the successive scan is higher than if no time is waited for which the currents remain low. At present time no detailed explanation exists about why Cu itself triggers this mechanism; it is not known even whether other elements can behave in a similar manner.

4.2.3 Behaviour of Pd on DL-97 layer

An example of the electrochemical behaviour of a DL-97 SAM which has been exposed to a Pd solution is shown in Figure 30. Of the three consecutive voltammograms the first one is distinctly different. Similar to the aldrithiol SAM a peak is evident only in the cathodic sweep

of the first cycle whereas the anodic sweep is featureless. The peak at -0.8 V is absent in the subsequent sweeps which indicates that the coordinated Pd was discharged during the first cycle. The subsequent scans are difficult to interpret as they are relatively featureless. Their overall shape is likely to be determined by different processes such as hydrogen adsorption onto the nanoparticles, since its potential is close to the one necessary to trigger this phenomenon. It is noted that Au/mica substrates show a very similar behaviour. Since they are significantly more costly than Au/Si substrates, these were used in most experiments. Au/mica was only used in experiments where the flatness is crucial such as in AFM imaging.

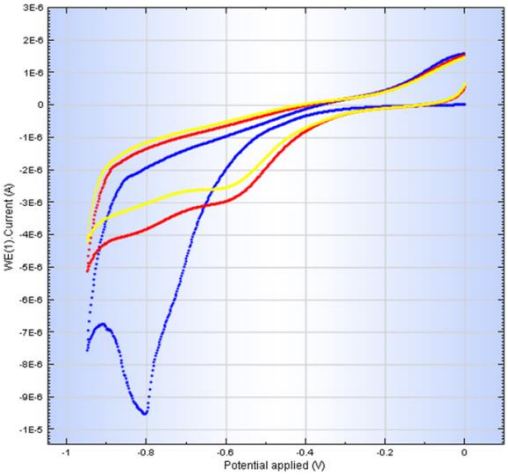

Figure 30: The first three cyclic voltammograms of a DL-97 SAM on Au/Si substrate with Pd-ions coordinated on top of the SAM. 0.1 M sulfuric acid as electrolyte and Pt reference electrode. Three consecutive cycles are shown, starting from 0 V. Scan rate 20 mV/s. Scans are in the order: blue, red, yellow. There is a significant difference between the behaviour of the first cycle and the behaviour of the successive cycles, evidencing that an irreversible phenomenon has happened.

4.2.4 Layer penetration tests

To test what the effect of the pyridine tail group in DL-97 is it is useful to perform analogous experiments with a structurally similar but chemically inert molecule. The molecule available is BP3 (shown in Figure 19) which is structurally analogous to DL-97 but differs from it only in the terminal part as the pyridine is substituted by a para-toluene moiety. Consequently it exhibits very similar structures including defects. The aim of this control experiment is as follows: if DL-97 were penetrable to ions, their voltammetric contribution would be also present with BP3. Instead, if DL-97 were impenetrable to ions only the contribution of ions coordinated and reduced on top of the DL-97 SAM would appear, while, because BP3 cannot coordinate ions, no signal would be visible in the voltammogram.

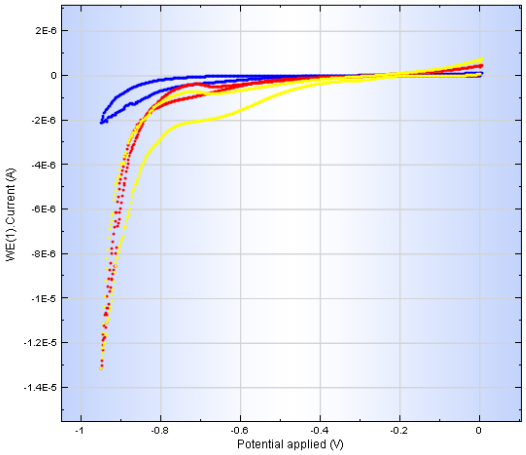

Figure 31: Cyclic voltammogramme of a BP3 SAM on Au/Si in 100 µM $PdSO_4$ in H_2SO_4 as electrolyte and with a Pt reference electrode. First 3 cycles are shown starting at 0 V and reversing at -0.95 V. Scans are in the order: blue, red, yellow.

The distinct influence of the pyridine moiety is documented by the graph displayed in Figure 31 which shows CVs of a SAM of BP3 in an acidic $PdSO_4$ electrolyte. It is clearly visible that essentially no reaction goes on, unless at very negative potentials where hydrogen evolution occurs. At these potentials ions may penetrate the SAM because of the increasing electric field, particularly at defects in the SAM which are always present at low concentration. Pd deposition at the SAM/substrate interface might affect the structural quality of the SAM and result in an

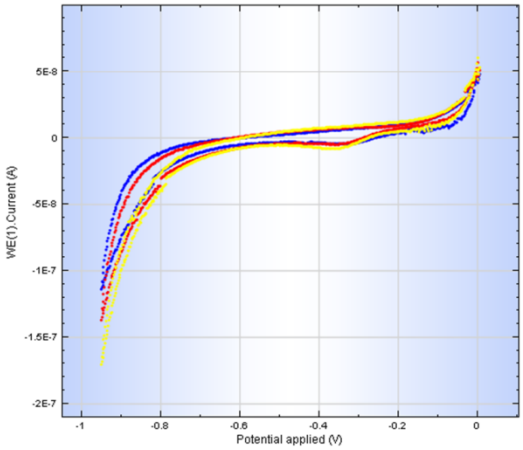

Figure 32: Cyclic voltammogramme of BP3 on Au/Si substrate in 0.1 M H_2SO_4 as electrolyte and a Pt reference electrode. 3 CVs are shown starting from 0 V and reversing at -0.95 V. Scans are in the order: blue, red, yellow.

increase of the hydrogen evolution in the second and subsequent cycles. The role of Pd becomes clear by a control experiment using only sulfuric acid as electrolyte. It may be suspected that also sulfuric acid penetrates the SAM, but an experiment analogous to the one just described which is shown in Figure 32, excludes this possibility because currents are about two orders of magnitude smaller than in the presence of Pd ions. In addition there is only a small increase in current upon multiple cycles. Beside interferences born by the electrolyte composition, it is possible that, if the time of exposition of the substrate covered by DL-97 to the Pd preparation solution was lengthened, penetration would go on to some extent, as it happens with aldrithiol SAMs. A more detailed study on this issue related to exposition time has not yet been carried out.

4.2.5 Generation of mixed nanoparticles

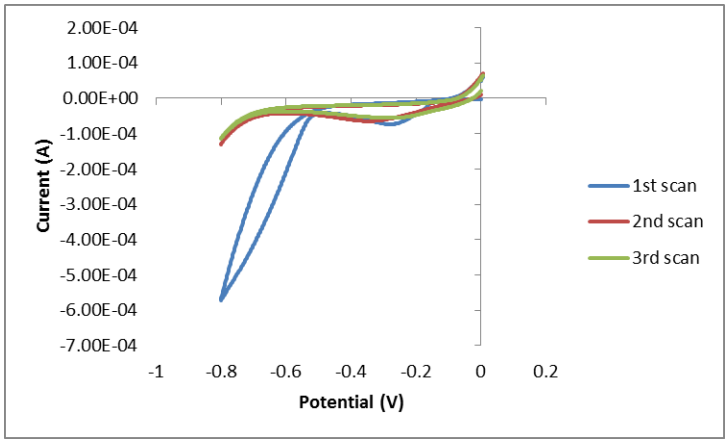

Figure 33: Cyclic voltammogram of DL-97 SAM on Au/Si with Pd coordinated on top in 1 mM $CuSO_4$ as electrolyte with Cu reference electrode. Only the first cycle of each of the 3 scans is displayed for clarity. Originally each scan was made up of 2 cycles. CVs start at 0 V. Scan rate is 20 mV/s. The first cycle of the first scan is completely different from all successive cycles of every scan, as evidence that an irreversible phenomenon has happened. The second and the third cycle are essentially equal to each other: this means that at that stage the electrochemical system doesn't change by much.

Also mixed Cu-and-Pd systems have been investigated: the general scheme to create mixed nanoparticles with these two elements involves Pd coordinated on top of DL-97 and Cu from solution. In this case it may be that the behaviour of the system follows the route of formation of a metal layer above the organic sublayer as described in section 4.2.2, or it may follow the route of formation of nanoparticles as described in section 4.2.3. In fact the second route goes on, and an example of the graph is outlined in Figure 33, in which, after a broad signal at moderately low potentials (between -0.2 V and -0.3 V), that can signify reduction of Cu from solution (as shown in Figure 29, Cu gets reduced around that potential) on top of the SAM that already coordinates Pd ions, a very strong feature appears beyond -0.5 V, a too positive potential to show hydrogen evolution (common reduction potentials tables display it at -0.827 V relative to SHE; however, it is dependent on pH); moreover, in the successive cycles, that signal is not present. STM studies reported in the literature prove that nanoparticles formed with a similar method, which involves only Pd but not Cu, once their nucleation is elicited,

grow only up to a certain size. It is suspected that the nanoparticles are passivated by hydrogen thus inhibiting further growth, even though it has not been proved unambiguously.[35] It seems that further electrochemical manipulation causes almost only density growth rather than size growth of the nanoparticles themselves. Again, the scans successive to the first one are difficult to interpret as no characteristic peaks appear and the features seen are likely to be associated with Cu deposition, including deposition of Cu nanoparticles at defects, and/or even capacitive current To summarize, it is clear that Pd has the ability to create nanoparticles as a consequence of electrochemical discharge, but a theoretical model to explain this phenomenon has still to be devised. Further investigations using, e.g., other metals would be useful to find an adequate explanation.

4.3 Pd promoted selective deposition of Cu

4.3.1 General remarks

This part of the project investigates whether selective electrodeposition of Cu on DL-97 SAMs is possible by Pd seeding. To test this a DL-97 SAM/Au substrate is partially immersed in a Pd solution as used above. In case of a contrast in the Cu deposition between Pd free and coordinated areas this proof of principle of selective deposition could be extended to patterning on the micro and nanometre scale by applying nanolithography and microcontact printing which are commonly used for applications that need well-defined structures such as electronic circuits.[60,61]

Half-dipping the DL-97 SAM/Au substrate in an incubation vial full of $PdSO_4$ solution creates two zones, one in which Pd is coordinated to the pyridine nitrogen of the SAM, and another one where the SAM is free of Pd. This conditioning of the substrate is crucial to see if the reduction of Cu ions from the electrolyte solution occurs preferentially on the Pd exposed areas. It is expected that charge transfer is facilitated by the presence of Pd nanoparticles. Thus, Cu deposition should occur much more easily on the Pd modified areas compared to areas of the native DL-97 SAM. Provided the potential is kept in a range where deposition occurs only in the zone covered by Pd, it should be possible to achieve selective deposition of Cu.

Deposition experiments are typically performed with a nucleation voltage at -0.3 V for 0.5 s, followed by a growth time at -0.15 V that lasts between 30 s and 60 s. The parameters can vary from experiment to experiment, but these are the most commonly used values. The nucleation step serves to create some nuclei on the substrate surface, the growth step serves to increase their size. The nucleation step uses a more negative potential which would cause a quite uniform nucleation of Cu on the whole area exposed to the electrolyte. The growth step instead uses a less negative potential. Such conditions allow deposition of Cu where Pd is present whereas in Pd-free areas the potential is not sufficiently negative for Cu deposition. Therefore, controlled deposition is achieved. While nucleation is more effective at negative potentials it has to be limited to short times in order to avoid nucleation at defects in the SAM layer. Once metallic nanoislands are formed further growth is performed at less negative potentials at which formation of new nuclei is suppressed. To summarize, the difference between areas with Pd and areas without Pd sits in the greater nucleation, since it determines if those zones will later

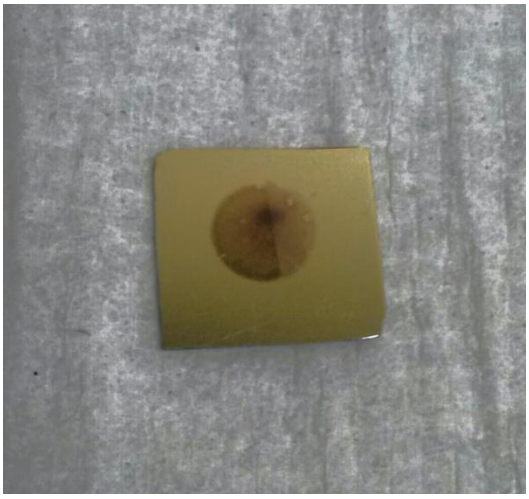

Figure 34: Preferential deposition of Cu on DL-97 SAM on Au/Si which has been partially exposed to Pd solution. Conditions of this sample are a nucleation step at -0.3 V for 0.05 s followed by a growth step at -0.15 V for 45 s in electrolyte 10 mM $CuSO_4$ with Cu reference electrode. The circular area has been exposed to the Cu electrolyte, the left half of the sample was exposed to $PdSO_4$ solution prior to the Cu deposition.

be covered or not covered with the growth step. Areas where Cu is deposited have a distinctly different colour from the yellow colour of the Au substrate. As seen with the bare eye and even better under the optical microscope, the mixed Cu-and-Pd deposits exhibit the reddish colour of Cu as illustrated in the left part of the circular area shown in Figure 34. Zones covered only by DL-97 show less heavy deposits (right half of circular area in Figure 34) and the colour is intermediate between the yellow of the Au substrate and more intense red of Cu-reddish of the Pd exposed left half. In order to optimise the contrast of deposition the overall growth time is varied. Since the zone covered by DL-97 and Pd already shows a good deposit by itself with these parameters it is of interest how a change in the growth time affects the contrast.

Growth times investigated are between 50 s and 30 s. A growth time of 50 s yields good deposits, whereas a growth time of 40 s leads to a poor coverage, because the surface appearance is much closer to experiments with a growth time of 30 s than to experiments with 50 s as growth time. Indeed, the experiment of Figure 34 shows a coverage of exceptional quality for a time above 40 s which is already obvious to the bare eye and even more so under the optical microscope. This signifies that between 40 s and 50 s growth time there is a burst in the visibility of the deposit. This does not mean that for growth times shorter than 40 s there is no growth, but it means that the crystals are too small to be seen or their density is too low. Analysing the charge by integrating the current of the chronoamperometric graph, an approximately linear increase is observed after about 25 s, (Figure 35 C), and, with it, according to Faraday's law, also the amount deposited on the electrode. Up to a certain point the deposited Cu crystals are sufficiently small and separated from each other so that reflection of light is dominated by the Au substrate. Above a certain size of the metal deposit, the colour is determined by reflection from the Cu crystals.

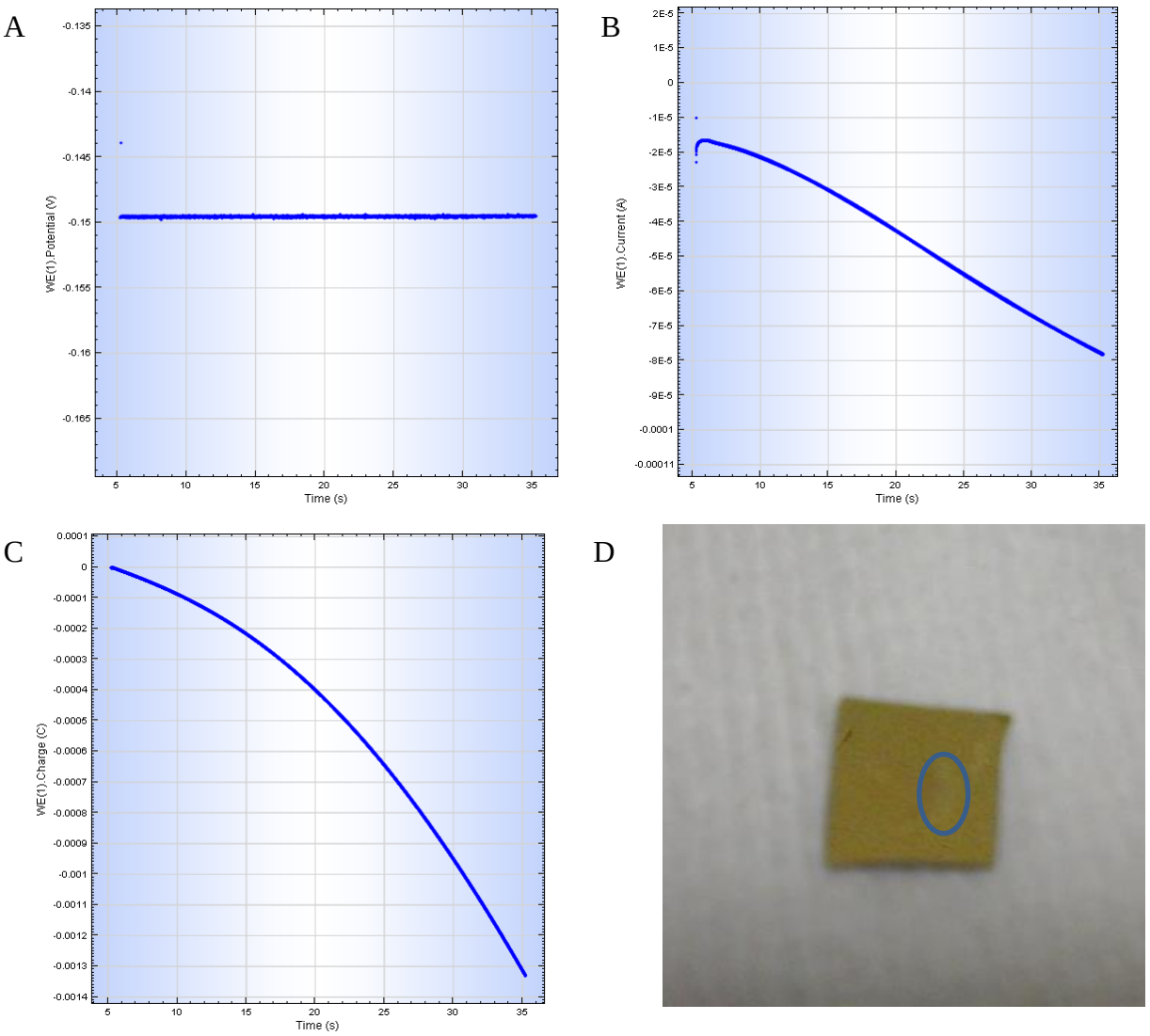

Figure 35: Chronoamperometry of Cu deposition on Pd coordinated DL-97 SAM/Au. Potential vs time (A), current-vs-time (B), charge-vs-time graphs (C) and image of the sample (D). Half-dipping is present, and a weakly covered area is labeled in the oval in picture D. Electrolyte is acidic 10 mM $CuSO_4$. The procedure comprises a nucleation step at -0.4 V (vs Cu) for 0.01 s and a growth step at -0.15 V for 30 s. In A the very short nucleation step is visible at the beginning of the graph. Also B shows a discontinuity at the start, due to the voltage steps. C displays instead a continuous increase in deposited charge, without abrupt changes. The graphs do not start exactly at 0 s because the instrument software does not set the beginning at that point, but somewhat later.

Further experiments are conducted along a direction complementary to the variation of growth time which is the variation of the nucleation time. It is known that, if the nucleation time is long (e.g. 0.5 s), many nuclei will form, that grow in the subsequent step of the procedure. Conversely, if the nucleation time is short (e.g. 0.1 s), fewer nuclei will form and yield a lower coverage. Indeed, the coverage of the substrate with Cu after the same growth times is higher for samples that have undergone a long nucleation time than for samples that have undergone a short nucleation time. Nevertheless, the optical microscope reveals an important characteristic of this kind of system: samples that undergo a short nucleation time grow more uniformly, showing at the optical microscopy a relatively lower degree of defects. This suggests a way to explain their growth tendency: when few nuclei are formed, they tend to grow more uniformly because the generated nuclei have approximately the same size; conversely, when many nuclei are formed, their size will vary to a greater extent and their

aspect will be less uniform. Of course, deposits triggered by a short nucleation time will grow less fast, but it is a matter of seconds. Under normal conditions, a uniform deposit is frequently required, hence the best way to obtain it is to impose a short nucleation time followed by a growth time as long as necessary, to be tailored to the required properties. Experiments of half-dipping substrates in the incubation vial have been carried out, and display (Figure 34) a clear partition line that divides the area initially covered only by DL-97 and the area initially covered by both DL-97 and Pd. The two zones are distinguishable based on the colour: pale orange for the former, reddish for the latter. The contrast between the area with Pd and the Pd-free area depends on the amount of substance deposited: while in the latter the deposition is almost negligible because Pd is absent that promotes deposition, in the former the deposition is as evident as effective are the nucleation and growth steps. Nevertheless, it is better not to push the potential of the steps excessively, or deposition will be initiated to some extent also on the Pd-free area, that is not desired.

4.3.2 Modifications in the experimental approach

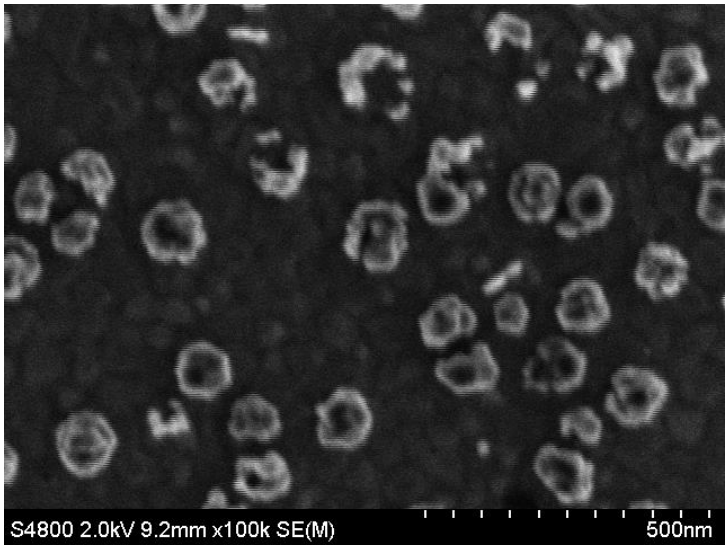

Figure 36: SEM image of a Au/Si substrate covered by DL-97 and half-immersed in a 100 µM $PdSO_4$ solution for 8 minutes before Cu deposition using a nucleation step at -0.3 V vs Cu for 0.05 s followed by a growth step at -0.15 V for 45 s. Electrolyte acidic 10 mM $CuSO_4$.

When the experiments of Pd promoted deposition produced reproducible results, SEM images of selected samples were taken. In Figure 36 an amount corresponding to an overall charge of 11 mC has been deposited on the substrate which is equivalent to a little more than 200 monolayers of Cu. This was calculated using equation 2, in which AW is the atomic weight of Cu, n_e is 2, ρ is 8.96 g/cm^3 and A is half of the area encompassed by the O-ring, $1.4135 \cdot 10^{-5}$ m^2. For this deposition the grains are quite far from being tightly packed. This is surprising as macroscopically a distinct Cu colour is seen, i.e., the colour of the Au substrate seems to be suppressed. This observation suggests that one has to be cautious in the interpretation of the optical images as regards the Cu coverage.

To investigate this finding further, various control experiments are carried out without dipping into Pd solution but changing deposition parameters. In chronoamperometric experiments such as those shown in Figure 35 deposition charge is measured which is unexpectedly high for a DL-97 SAM without coordinated Pd. At the potentials the SAM without Pd should be rather passivating and, thus, Cu should not be massively deposited. Hence, it is suspected that Cu somehow penetrates the DL-97 layer even though this is surprising considering the rigidity of the aromatic rings of the DL-97 layer. If the potential were way more cathodic, the electric field would be so strong to induce Cu ions to penetrate the layer, but at the values applied here

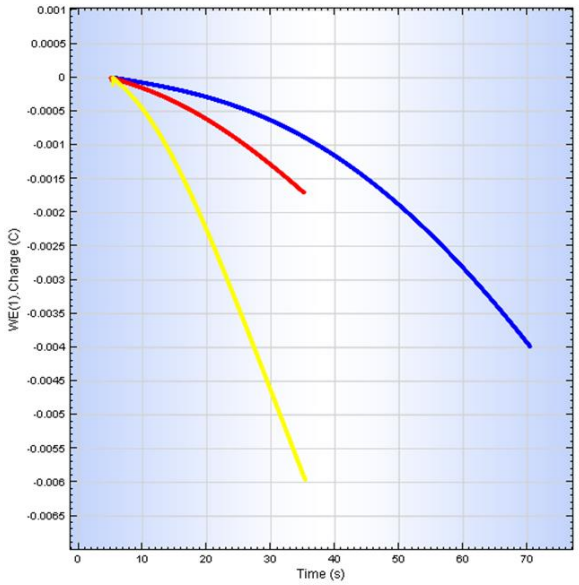

Figure 37: Charge-vs-time graph of Cu deposition on DL-97 SAM. Experiments performed without dipping the substrate in $PdSO_4$ vial and inserted in cell in that electrolyte is 10 mM $CuSO_4$ in H_2SO_4 with Cu reference electrode. Blue curve has a nucleation step of -0.25 V for 0.1 s and a growth step of -0.15 V for 65 s. Red scan has a nucleation step of -0.35 V for 0.1 s and a growth step of -0.15 V for 30 s. Yellow scan has a nucleation step of -0.4 V for 0.1 s and a growth step of -0.15 V for 30 s.

it should not happen to that extent (the experimented potential highest in absolute value is just -0.4 V).

A crucial point related to this issue is the preparation of the samples. When DL-97 layers are prepared by immersion of Au/Si substrates into the DL-97 solution at room temperature, the resulting structure will be affected by different types of defects. These can be conformational defects or contaminations incorporated into the SAM. They are usually present to some extent and are difficult to be completely eliminated. Gauche defects in the alkane spacer chains of the thiol molecules can produce ill-orientated molecules with the aromatic part of the molecule even touching the Au substrate instead of being directed towards the solution. This non-ideal structure seems realistic and explains perfectly that Cu ions can penetrate into the DL-97 layer and are reduced at the SAM-substrate interface. Folded chains are less effective as a barrier, because the aromatic moieties do not exhibit the ideal dense packing which prevents Cu ions from penetrating.

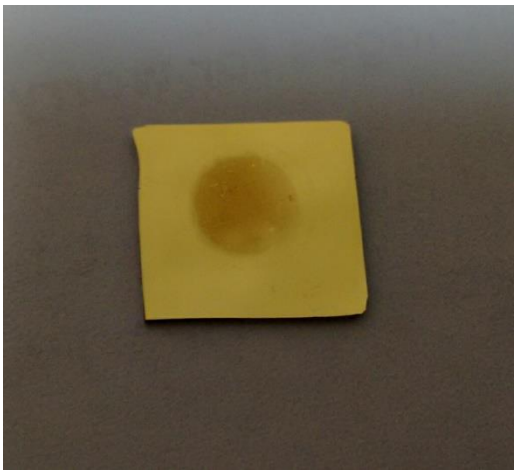

Figure 38: Example of substrate resulting from an experiment in which the reference wire has been distanced from the substrate surface by 6-7 mm. This sample undergoes a nucleation step at -0.4 V for 0.01 s with an interval time of 0.0025 s followed by a growth step at -0.15 V for 30 s with an interval time of 0.01 s in electrolyte 10 mM $CuSO_4$ with Cu reference electrode.

To reduce this problem, DL-97 SAMs were prepared at elevated temperature by keeping samples immersed in DL-97 solution in an oven overnight (~16 h) at a temperature between 60 °C and 65 °C. Under these conditions the chain should unfold, thus, yielding a SAM of higher structural quality.

At this point an important note regarding the position of the capillary with the reference electrode is made. If Figure 34 is inspected, a clear dark spot can be observed near the centre of the deposition area, like an accumulation of reduced Cu that seems to be located just below the capillary containing the reference wire. This is not desirable since an ideal deposit should be as uniform as possible. This feature may be explained in the following way. If the reference wire inside the capillary is too close to the working electrode, even though its purpose is only to sense the potential of the working electrode, it can affect to some extent the ongoing electrochemical reaction. For example,

confining the space between capillary and substrate a preferential deposition below the reference wire itself might result. Increasing the distance between the substrate and the reference wire to 6-7 mm while keeping the capillary in the same position solves the problem. Successive experiments performed under the same conditions but with this modification show a significantly more uniform coverage (see Figure 38). However, it seems that, the higher the applied potential is, the more the reference wire has to be distant from the substrate surface.

An accurate study about the relation between this distance and the voltage applied to the cell has not been carried out because it is not the purpose of this work. However, for the potential used in the present experiments (fractions of V in absolute value), this retraction is overall sufficient. Also a detailed study about the influence of the temperature in the preparation of the samples has not been carried out because it went beyond the objectives of this work; optimal conditions were reached and accepted without further studies, provided the whole procedure worked finely.

Besides the influence of defects in the SAM, the question arises what other factors might affect the deposition such as the presence of oxygen. Therefore, a comparison of the deposition with oxygen present in the electrolyte (as in the experiments presented so far) with deposition in an N_2 purged electrolyte. Purging was done for ~20 minutes through a tube inserted through a hole in the top cap of the cell, before it is stopped just before the Cu deposition. Also experiments were performed without discontinuing the purging during electrochemical deposition, as well as experiments in which purging cable is present but inactive to check if its presence itself triggers anything. As a result, neither in the chronoamperometric graphs nor in the appearance of the visible deposit a significant difference between purged and non-purged electrolyte was seen.

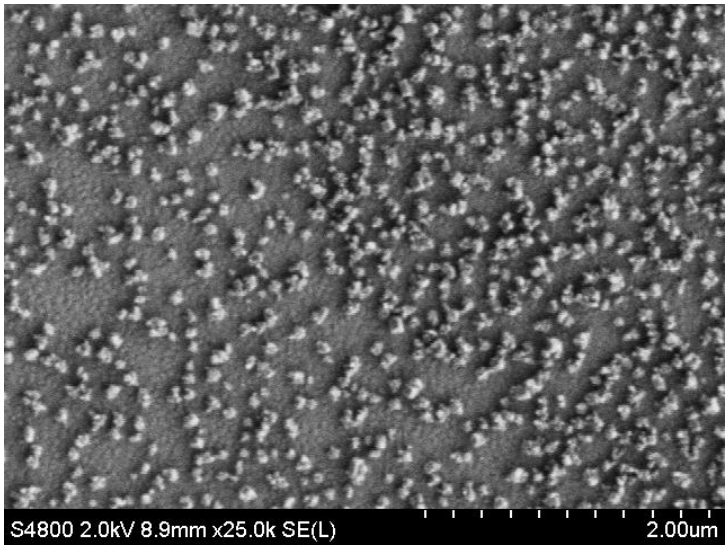

Figure 39: SEM image of a Au/Si substrate covered by DL-97 and immersed in 100 µM $PdSO_4$ solution that undergoes a nucleation step at -0.4 V for 0.01 s with an interval time of 0.0025 s followed by a growth step at -0.15 V for 30 s with an interval time of 0.01 s in electrolyte 10 mM $CuSO_4$ with Cu reference electrode. As soon as the scan is finished, electrolyte is drawn out with a pipette and the remainder is diluted with ultra-pure water.

However, one point to consider is that, due to the small amounts of Cu deposited, immediately after the end of the scan, the acidic solution inside the cell may affect the just formed deposit. Noting that Cu can form oxides which then are dissolved in an acidic environment an oxygen containing electrolyte of about pH 1 as used in the experiments can reduce the amount of deposited Cu. Thus, experiments are performed in which immediately after the deposition the acidic electrolyte is removed with a pipette, and, as quickly as possible, replaced by ultra-pure water to dilute thoroughly the small quantity of acid that remains, and, after these swift additional actions, the cell is dismounted and the substrate is analysed as usual.

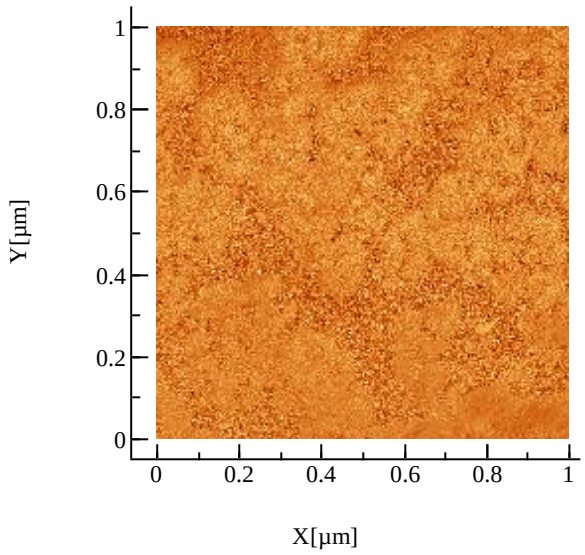

Figure 40: A 1 µm·1 µm AFM image that shows how the deposition on the substrate is regular. Sample is the same as in Figure 39. Difference in height among zones is not excessive. Colour similarity corresponds to height similarity.

As confirmation of the utility of these additional actions, the deposition on new substrates appears more pronounced upon inspection even at bare eye, and SEM and AFM yield images of their surface on that Cu grains are visibly more tight-packed (Figure 39 and Figure 40).

Normally, the deposition procedure comprises a nucleation step followed by a growth step, whose potentials and durations can vary depending on the experiment. All curves that ensue from this procedure scheme show, at the start, a parabola-like behaviour (Figure 35 C and Figure 37), even though on a short interval it is quite difficult to spot the exact dependence, and the exponent of the power may be higher than just 2, and, for the last part of the scan, it seems to follow a linear trend (this tendency is visible especially for long growth times). In an experiment with only a long period at a low deposition potential (the "growth step") and no short period at a more negative potential (the "nucleation step") the result was a linear trend that starts right from the beginning of the deposition. Alternatively, this low current may be interpreted as a side-reaction of some sort, whose possible nature is unknown. The charge-vs-time graph is presented in Figure 41 A, in which the very low value of the developed charge is clearly observable. This seems to suggest that a polynomial law is the key to understand the overall deposition process. It seems also that higher order terms become less and less important as time proceeds while the linear term takes over. The fact that the nonlinear term is negligible if the "nucleation step" is not present points to a relation between the parabolic term and the formation of crystallization centres: tentatively, it can be explained by assuming that the parabolic term reflects the rate of formation of new nuclei on

A

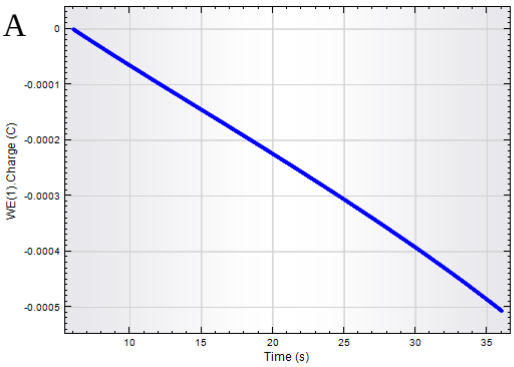

B

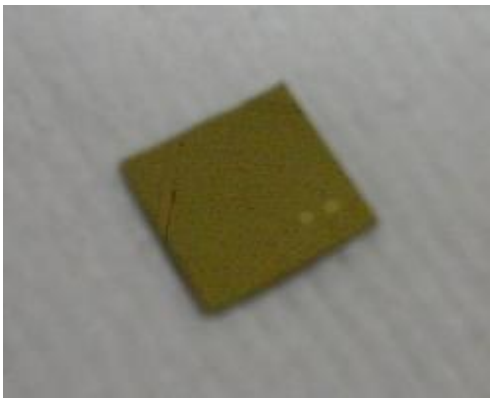

Figure 41: Charge-vs-time graph (A) and picture of the sample itself (B) of an experiment performed without half-dipping the substrate in 100 µM $PdSO_4$ solution in which only the growth step is present, that is, a low voltage in absolute value applied for a long time lag. In cell electrolyte is 10 mM $CuSO_4$, there is Cu reference electrode, voltage is -0.15 V and is applied for 30 s, with an interval time of 0.01 s. Charge developed is very low (less than 1 mC in absolute value), and, consequently, the sample does not look very covered.

the substrate and the linear term measures the rate of growth of nuclei. However, if conditions are such that nuclei are not formed in the initial stage, a certain number of nuclei will form also during the "growth step". This number is, however, low compared to the one of the nucleation step. The interpretation of the two terms involved in electrodeposition dynamics makes sense also from a practical point of view: if the substrate surface gets more and more covered, the free area available for the formation of new nuclei is reduced and the process is increasingly dominated by the growth of already existing crystals, i.e., the linear term dominates, as is clearly visible in the terminal part of the experiments shown in Figure 36. Unfortunately, an exact law cannot be devised at this point because the SAM controlled electrodeposition depends on many parameters, not only on the ones that have been discussed in the analysis above: nucleation potential, nucleation time, growth potential, growth time, quantity of defects on the substrate surface, quality of defects on the substrate surface, purity of chemicals in use, degree of coverage reached up to a certain stage of the experiment to name the most obvious ones.

As already stated, works regarding deposition of metals or metal compounds above an organic sublayer are few: to be noticed is a work of deposition of ZnO on Cu phthalocyanine and pentacene by Cruickshank et al.,[62] but their publication does provide an equation to quantitatively describe this type of process. Staikov suggests that the electrochemical system under examination has to overcome a barrier called "nucleation work" that represents the energy excess that opposes the formation of a new nucleus. In brief, because a small new nucleus has a rather high surface energy its generation is unfavourable. Therefore, a fluctuation of sufficient energy is needed to exceed the critical size above which a nucleus becomes stable. In case of stationary nucleation, that is, when the nucleation rate J(t) is constant and indicated with J_0, the following equation holds

$$J_0 = \frac{Z_0 W}{\lambda} e^{-\frac{\Delta G(n_C)}{k_B T}} \qquad (4)$$

here Z_0 represents the surface density of active sites (the zones on which nucleation can go on) on the substrate, W is the frequency of attachment of single atoms on the surface of the sample, λ is Zeldovich's factor and is relative to the supersaturation of the solution, $\Delta G(n_c)$ is the energy barrier (n_c is the critical number of atoms that compose the nucleus) discussed above, k_B is Boltzmann's constant and T is temperature.[63] In its basic principles and within the limitation imposed by the experimental conditions, equation 4 is valid even though it remains to be seen to what extent the equation holds also for the deposition on a SAM of the type presented in this work. Georgi Staikov supports these conclusions with experiments on crystal metal electrodes, but an organic SAM may be quite different, for several reasons. To start with, a metal surface is impenetrable, while SAMs are not, as learnt above, and mushrooms can arise from inside the SAM itself. Mushroom growth follows dynamics quite different from either nanoislands growth or layer-by-layer growth. In addition, the upper surface of a SAM is less definite than the one of a crystal metal electrode, and the concept of crystallographic mismatch, that is the basis for the distinction between Frank-van der Merwe and Stranski-Krastanov growth mechanism, is partially different because the interaction between metal and SAM is weaker. Furthermore, the growth of metal clusters could alter to some extent either the topography or

the physical-chemical properties of the sublayer itself, as was demonstrated through a study performed with X-ray photoelectron spectroscopy on a system analogous to the one of the present research work but in which the SAM showed a carboxylic tail group.[64] These facts altogether demonstrate that the presence of SAM between metal electrode and deposited overlayer changes dramatically the system under study, and equation 4 may not exactly hold for this kind of systems. At this point a quantitative understanding of the electrodeposition of metal on top of a SAM seems far from being fully unveiled.

5 Future work

The project demonstrated the principle feasibility that copper deposition can be promoted by Pd nuclei generated on top of a SAM. The contrast in Cu deposition between Pd-coordinated and Pd free areas opens the possibility of patterning. Since SAMs can be patterned from the nanometre to the micrometre range by a range of techniques such as microcontact printing or e-beam lithography it will be interesting to explore on what length scale the generation of metal patterns on top of a SAM might be possible.

Another point is a better understanding of the deposition mechanism which has to involve analysis at the smallest scale possible. To achieve this, in future selective deposition on Au/mica samples should be attempted which, in contrast to the Au/Si substrates used in this work, exhibit extended atomically flat terraces. Up to now analysis with non-optical microscopy like SEM and AFM have been performed, but in the future STM should be applied as well due to its superior resolution. It is hoped that these experiments on the electrodeposition of metal on SAMs improve the knowledge in the field to the extent that a quantitative description becomes possible.

6 Endnotes

[1] Nuzzo R. G., Allara D. L., J. Am. Chem. Soc., 4481, *105*, 1983
[2] T.-L. Ho, The Hard Soft Acids Bases (HSAB) Principle and Organic Chemistry, Chem. Rev., 1-20, *75(1)*, 1975
[3] Hasan M., Bethell D., Brust M., J. Am. Chem. Soc., 1132, *124*, 2002
[4] Widrig C. A., Chung C., Porter M. D, J. Electroanal. Chem. Interfacial Electrochem., 335, *310*, 1991
[5] Zhong, C.-J., Woods N. T., Dawson B. G., Porter M. D., Electrochem. Commun., 17, *1*, 1999
[6] Andreoni W., Curioni A., Gronbeck H., Int. J. Quantum Chem., 598, *80*, 2000
[7] Noh J., Murase T., Nakajima K., Lee H., Hara M., J. Phys. Chem., 7411, *104*, 2000
[8] Noh J., Nakamura F., Kim J., Lee H., Hara M., Mol. Cryst. Liq. Cryst., 165, *377*, 2002
[9] Thorsten Baunach, Valentina Ivanova, Dieter M. Kolb, Hans-Gerd Boyen, Paul Ziemann, Michael Büttner, Peter Oelhafen, A New Approach to the Electrochemical Metallization of Organic Monolayers: Palladium Deposition onto a 4,4'-Dithiodipyridine Self-Assembled Monolayer, Advanced Materials, 2024-2028, *16*, 2004
[10] Dubois L. H., Nuzzo R. G., Synthesis, Structure and Properties of Model Organic Surfaces, Annu. Rev. Phys. Chem., 437, *43*, 1992
[11] http://www.sigmaaldrich.com/technical-documents/articles/material-matters/self-assembled-monolayers.html accessed on 29 January 2015
[12] Esplandiu M. J., Noeske P. L. M., XPS investigations on the interactions of 1,6-hexanedithiol/Au(111) layers with metallic and ionic silver species, Applied Surface Science, 166-182, *199*, 2002
[13] J. Scharf, H.-H. Strehblow, B. Zeysing, A. Terfort, Electrochemical and surface analytical studies of self-assembled monolayers of three aromatic thiols on gold electrodes, Journal of Solid State Electrochemistry, 396-401, *5*, 2001

[14] Yufei M., Min Z., Mingwu B., Preparation and nano/microtribological properties of perfluorododecanoic acid (PFDA)–3-aminopropyltriethoxysilane (APS) self-assembled dual-layer film deposited on silicon, Colloids and Surfaces A: Physicochemical and Engineering Aspects, 170-176, *322*, 2008
[15] Costelle L., Lind L., Jalkanen P., Raisanen M. T., Nowak, R., Raisanen J., Conventional Nanoindentation in Self-Assembled Monolayers Deposited on Gold and Silver Substrates, Journal of Nanomaterials, Article ID 585123, 2012
[16] Holmlin R. E., Haag R., Chabinyc M. L., Ismagilov R. F., Cohen A. E., Terfort A., Rampi M. A., Whitesides G. M., Electron transport through thin organic films in metal-insulator-metal junctions based on self-assembled monolayers, Journal of the American Chemical Society, 5075-5085, *123*, 2001
[17] Shubha H. N., Venkatesha T. V., Vathsala K., Pavitra M. K., Kumar M. K. P., Preparation of Self Assembled Sodium Oleate Monolayer on Mild Steel and Its Corrosion Inhibition Behavior in Saline water, ACS Applied Materials & Interfaces, 10738-10744, *5*, 2013
[18] Dannenberger O., Wolff J. J., Buck, M., Langmuir, 4679, *14*, 1998
[19] Bain C. D., Troughton E. B., Tao Y. T., Evall J., Whitesides G. M., Nuzzo R. G., J. Am. Chem. Soc., 321, *111*, 1989
[20] Yamada R., Sakai H., Uosaki K., Chem. Lett., 667, 1999
[21] Bensebaa F., Voicu R., Huron L., Ellis T. H., Kruus, E. Langmuir, 5335, *13*, 1997
[22] Bain C. D., Troughton E. B., Tao Y.-T., Evall J., Whitesides G. M., Nuzzo R. G., Formation of Monolayer Films by the Spontaneous Assembly of Organic Thiols from Solution onto Gold, Journal of American Chemical Society, 321-335, *111*, 1989
[23] Himmelhaus M., Eisert F., Buck M., Grunze M., Self-assembly of n-alkanethiol monolayers. A study by IR-visible sum frequency spectroscopy (SFG), Journal of Physical Chemistry B, 576-584, *104*, 2000
[24] N. Nishida, M. Hara, H. Sasabe, W. Knoll, Thermal Desorption Spectroscopy of Alkanethiol Self-Assembled Monolayer on Au(111), Japanese Journal of Applied Physics, 5866, *35*, 1996
[25] Thom I., Buck M., Electrochemical stability of self-assembled monolayers of biphenyl based thiols studied by cyclic voltammetry and second harmonic generation, Surface Science, 33-46, *581*, 2005
[26] Gorman C. B., Biebuyck H. A., Whitesides G. M., Langmuir, 2242, *11*, 1995
[27] J. Garside, A. Barnum, K. Nelson, C. Martinez, N. Le, K. Monahan, N. Bui, D. Roeuth, K. Slowinski, Electron Tunneling through Monolayers of α,ω-thioalkanoic acids in Hg-Hg Electrochemical Tunnel Junctions in Water, Int. J. Electrochem. Sci., 4345-4351, *9*, 2014
[28] R. L. Mc Creery, The merger of electrochemistry and molecular electronics, The chemical record, 149-163, *12*, 2012
[29] H. Haick, D. Cahen, Making contact: Connecting molecules electrically to the macroscopic world, Progress in Surface Science, 217-261, *83*, 2008
[30] Rampi M. A., Whitesides G. M., A versatile experimental approach for understanding electron transport through organic materials, Chemical Physics, 373-391, *281*, 2002
[31] Muglali M. I., Liu J., Bashir A., Borissov D., Xu M., Wang Y., Wöll C., Rohwerder M., On the complexation kinetics for metallization of organic layers: palladium onto a pyridine-terminated araliphatic thiol film, Physical Chemistry Chemical Physics, 4703-4712, 14, 2012
[32] Shekhah O., Busse C., Bashir A., Turcu F., Yin X., Cyganik P., Birkner A., Schuhmann W., Wöll C., Electrochemically deposited Pd islands on an organic surface: the presence of Coulomb blockade in STM I(V) curves at room temperature, Physical Chemistry Chemical Physics, 3375-3378, *8*, 2006
[33] Halik M., Klauk H., Zschieschang U., Schmid G., Dehm C., Schütz M., Maisch S., Effenberger F., Brunnbauer M., Stellacci F., Low-voltage organic transistors with an amorphous molecular gate dielectric, Nature, 963-966, *431*, 2004
[34] Manolova M., Kayser M., Kolb D. M., Boyen H.-G., Ziemann P., Mayer D., Wirth A., Rhodium deposition onto a 4-mercaptopyridine SAM on Au(1 1 1), Electrochimica Acta, 2740-2745, *52*, 2007
[35] Silien C., Lahaye D., Caffio M., Schaub R., Champness N. R., Buck M., Electrodeposition of Palladium onto a Pyridine-Terminated Self-Assembled Monolayer, Langmuir, 2567-2574, *27*, 2011
[36] Chen D., Cui P., Liu H., Heterogeneous nanocomposites composed of silver sulfide and hollow structured Pd nanoparticles with enhanced catalytic activity toward formic acid oxidation, Electrochimica Acta, 461-467, *153*, 2015
[37] http://en.wikipedia.org/wiki/Cyclic_voltammetry accessed on 26 August 2014
[38] http://staff.tanta.edu.eg/uploads/ch37.pdf accessed on 9 March 2015
[39] http://www.ceb.cam.ac.uk/research/groups/rg-eme/teaching-notes/linear-sweep-and-cyclic-voltametry-the-principles accessed on 26 August 2014
[40] http://en.wikipedia.org/wiki/Randles%E2%80%93Sevcik_equation accessed on 26 August 2014
[41] http://serc.carleton.edu/research_education/geochemsheets/techniques/SEM.html accessed on 8 December 2014
[42] http://en.wikipedia.org/wiki/Scanning_electron_microscope accessed on 26 February 2015

[43] http://www.vias.org/physics/example_6_4_02.html accessed on 5 December 2014
[44] http://www.purdue.edu/ehps/rem/rs/sem.htm accessd on 8 December 2014
[45] http://en.wikipedia.org/wiki/File:AFM_Nanoscope_IIIa.jpg accessed on 9 December 2014
[46] http://en.wikipedia.org/wiki/Atomic_force_microscopy#mediaviewer/File:Atomic_force_microscope_block_diagram.svg accessed on 9 December 2014
[47] http://web.physics.ucsb.edu/~hhansma/biomolecules.htm accessed on 9 December 2014; the image is cropped to encompass only the right part
[48] T. J. Guenther, M. Suhr, J. Raff, K. Pollmann, Immobilization of microorganisms for AFM studies in liquids, RSC Advances, 51156-51164, *4*, 2014
[49] https://en.wikipedia.org/wiki/Atomic_force_microscopy#Non-contact_mode accessed on 3 September 2015
[50] http://callistosoft.narod.ru/English/Home.htm accessed on 25 November 2014
[51] http://gwyddion.net/ accessed on 25 November 2014
[52] I. Horcas, R. Fernandez, J. M. Gomez-Rodriguez, J. Colchero, J. Gomez-Herrero, A. M. Baro, WSXM: A software for scanning probe microscopy and a tool for nanotechnology, Review of Scientific Instruments, Article Number 013705, *78*, 2007
[53] H. Philippe, E.-K.-C. Sofiane, A. Beaussart, J. A. Gheoghegan, T. J. Foster, Y. F. Dufrene, The binding force of the staphylococcal adhesin SdrG is remarkably strong, Molecular Microbiology, 356-368, *93*, 2014
[54] M. Lanza, T. Gao, Z. Yin et al., Nanogap based graphene coated AFM tips with high spatial resolution, conductivity and durability, Nanoscale, 10816-10823, *5*, 2013
[55] K.-H. Chung, D.-E. Kim, Wear characteristics of diamond-coated atomic force microscope probe, Ultramicroscopy, 1-10, *108*, 2007
[56] http://en.wikipedia.org/wiki/Atomic_force_microscopy accessed on 27 February 2015
[57] C. R. Brundle, C. A. Evans jr., S. Wilson, Encyclopedia of Materials Characterization, Manning Publications Co., 85-98, 1992
[58] Silien C., Buck. M.; Goretzki G., Lahaye D., Champness N. R., Weidner T., Zharnikov M., Self-assembly of a pyridine-terminated thiol monolayer on Au(111), Langmuir, 959–967, *25*, 2009
[59] H.-T. Rong, S. Frey, Y. J. Yang, M. Zharnikov, M. Buck, M. Wühn, C. Wöll, and G. Helmchen, On the Importance of the Headgroup Substrate Bond in Thiol Monolayers: A Study of Biphenyl-Based Thiols on Gold and Silver, Langmuir, 1582–1593, *17*, 2001
[60] K. Piglmayer, R. Denk, D. Bäuerle, Laser-induced surface patterning by means of microspheres, Applied Physics Letters, 4693-4695, *80*, 2002
[61] J. A. Rogers, Z. Bao, A. Makhija, P. Braun, Printing Process Suitable for Reel-to-Reel Production of High-Performance Organic Transistors and Circuits, Advanced Materials, 741-745, *11*, 1999
[62] A. C. Cruickshank, S. E. R. Tay, B. N. Illy, R. da Campo, S. Schumann, T. S. Jones, S, Heutz, M. A. Mc Lachlan, D. W. Mc Comb, D. J. Riley, M. P. Ryan, Electrodeposition of ZnO Nanostructures on Molecular Thin Films, Chemistry of Materials, 3863-3870, *23*, 2011
[63] G. Staikov, Electrocrystallization in Nanotechnology, WILEY-VCH Verlag GmbH & Co. KGaA, 10-11, 2007
[64] C. M. Whelan, J. Ghijsen, J.-J. Pireaux, K. Maex, Cu adsorption on carboxylic acid-terminated self-assembled monolayers: a high-resolution X-ray photoelectron spectroscopy study, Thin Solid Films, 388-392, *464*, 2004